Atmospheric processing and aerosol aging responsible for observed increase in absorptivity of long-range transported smoke over the southeast Atlantic

Abdulamid A. Fakoya[1], Jens Redemann[1], Pablo E. Saide[2,3], Lan Gao[1], Logan T. Mitchell[1], Calvin Howes[3], Amie Dobracki[4], Ian Chang[5], Gonzalo A. Ferrada[6,7], Kristina Pistone[8,9], Sam E. Leblanc[8,9], Michal Segal-Rozenhaimer[8,9,13], Arthur J. Sedlacek III[4], Thomas Eck[10,11], Brent Holben[11], Pawan Gupta[11], Elena Lind[11], Paquita Zuidema[12], Gregory Carmichael[14,15] and Connor J. Flynn[1]

[1]School of Meteorology, University of Oklahoma, Norman, Oklahoma, USA

[2]Institute of the Environment and Sustainability, University of California, Los Angeles, Los Angeles, California, USA

[3]Department of Atmospheric and Oceanic Sciences, University of California, Los Angeles, Los Angeles, California, USA

[4]Environmental and Climate Sciences Department, Brookhaven National Laboratory, Upton, New York, USA

[5]Department of Earth, Environmental, and Geographical Sciences, The University of North Carolina at Charlotte, Charlotte, North Carolina, USA

[6]Cooperative Institute for Research in Environmental Sciences, University of Colorado, Boulder, Colorado, USA

[7]Global Systems Laboratory, National Oceanic and Atmospheric Administration, Boulder, Colorado, USA

[8]Bay Area Environmental Research Institute, Moffett Field, California, USA

[9]NASA Ames Research Center, Moffett Field, California, USA

[10]University of Maryland Baltimore County, Baltimore, Maryland, USA

[11]NASA Goddard Space Flight Center, Greenbelt, Maryland, USA

[12]Department of Atmospheric Sciences, Rosenstiel School, University of Miami, Miami, Florida, USA

[13]Department of Geophysics, Porter School of the Environment and Earth Sciences, Tel-Aviv University, Tel-Aviv, Israel

[14]Center for Global and Regional Environmental Research (CGRER), University of Iowa, Iowa City, Iowa, USA

[15]Department of Chemical and Biochemical Engineering, University of Iowa, Iowa City, Iowa, USA

Correspondence to: Abdulamid A. Fakoya (abdulamid.fakoya@ou.edu) and Jens Redemann (jredemann@ou.edu)

Formatted: Font color: Auto

Abstract.

Biomass burning aerosols (BBA) from agricultural fires in southern Africa contribute about one-third of global carbonaceous aerosol load. These particles have strong radiative effects in the southeast Atlantic (SEA), which depend in part on the radiative contrast between the aerosol layer in the free troposphere (FT) and the underlying cloud layer. However, there is large disagreement in model estimates of aerosol-driven climate forcing due to uncertainties in the vertical distribution, optical properties, and lifecycle of these particles.

This study applies a novel method combining remote sensing observations with regional model outputs to investigate the aging of the BBA and its impact on the optical properties during transatlantic transport from emission sources in Africa to the SEA. Results show distinct variations in extinction Ångstrom exponent (EAE) and single scattering albedo (SSA) as aerosol age. Near the source, fresh aerosols are characterized by low mean SSA (0.84) and high EAE (1.85), indicating smaller, highly absorbing particles. By isolating marine contributions from the total column during BBA transport across the SEA, our analysis reveals an initial decrease in BBA absorptivity, with mean FT SSA of 0.87 after 6–7 days, followed by increased absorptivity with mean FT SSA of 0.84 after 10 days, suggesting enhanced absorption due to chemical aging.

These findings indicate that BBA becomes more absorbing during extended transport across the SEA, with implications for reducing model uncertainties. Our remote sensing-based results agree well with previous in-situ studies and offer new insights into aerosol-radiation interactions and the energy balance over the SEA.

~~Biomass burning aerosols (BBA) primarily from agricultural fires across southern Africa account for approximately a third of carbonaceous particles in the global atmosphere. These particles have strong direct radiative effects over the southeast Atlantic (SEA), which depend on the radiative contrast between the aerosol layer residing in the free troposphere (FT) and the underlying cloud layer over the SEA. However, there are large disagreements in model estimates of aerosol-driven climate forcing due to uncertainties in the vertical distribution, optical properties, and lifecycle of these particles.~~

~~In this study, we introduce a novel method to extend the observational timescales for studying the lifecycle of atmospheric aerosols. Our approach integrates remote sensing observations from ground-based AERONET (AErosol RObotic NETwork) in the emission region and airborne 4STAR (Spectrometers for Sky-Scanning, Sun-Tracking Atmospheric Research) over the SEA, collected during the ORACLES (ObseRvations of Aerosols above CLouds and their intEractionS), with outputs from two region-specific model simulations, to investigate the aging of BBA and its impact on the optical properties during transatlantic transport, covering the entire pathway from emission sources within Africa to the SEA.~~

~~Results show distinct variations in Ångstrom exponent (AE) and single scattering albedo (SSA) as aerosol age. Near the burning regions, the youngest aerosols are characterized by low mean SSA of 0.84 and elevated AE values of 1.85, indicating smaller, highly absorbing BBA close to their source. Upon isolating marine aerosol contributions from the total column over the SEA, our analysis reveals a decrease in BBA absorptivity, with mean FT SSA of 0.87 after 6 – 7 days of transport, and a subsequent increased absorptivity over the ocean, reaching a mean FT SSA of 0.84 after 10 days.~~

These findings indicate that BBA becomes more absorbing during extended transport across the SEA, attributable to chemical aging processes in the FT. The 0.03 change in SSA documented in this study suggests that BBA transport and aging can have substantial implication for the local direct radiative effects of BBA in the SEA. Our remote sensing based results agree well with previous in situ studies and offer a new methodology for understanding BBA's evolution and provide new insights into aerosol-radiation interactions and their impact on the regional energy balance.

1 Introduction

Atmospheric aerosols play a crucial role in Earth's energy balance and climate system. Aerosols perturb the vertical temperature structure, altering the atmospheric stability and overall radiation balance through interactions with sunlight via scattering and absorption, known as aerosol-radiation interactions (ARI) (Ackerman et al., 2000; Boucher, 2015; Hansen et al., 1997; Koch & Del Genio, 2010; Samset et al., 2018; Santer et al., 1996). Aerosols also serve as cloud condensation nuclei (CCN) or ice-nucleating particles (INPs) that influence cloud microphysics and modify cloud reflectivity (Twomey, 1974, 1977) and lifespan (Albrecht, 1989) through aerosol-cloud interactions (ACI) (Ackerman et al., 2000; Boucher, 2015). The resulting impacts of ARI and ACI on climate are cumulatively quantified as climate forcing, and its magnitude and sign depend on various factors, including particle size, composition, concentration, mixing state, optical properties, and vertical distribution at a given location.

Single-scattering albedo (SSA), the ratio of aerosol scattering to aerosol extinction, an indicator of aerosol absorptivity, is an important parameter in deriving the radiative effects of aerosols (Bergstrom et al., 2007; Chylek & Wong, 1995; Satheesh et al., 2010; Takemura et al., 2002). Non-absorbing aerosols have SSA of 1, whereas absorbing aerosols have lower values (Moosmüller et al., 2012). The magnitude of the direct aerosol radiative effect depends on the interplay between the radiative properties of aerosols and the underlying scene (Chand et al., 2009; Keil & Haywood, 2003). Non-absorbing aerosols more effectively elevate the scene albedo in regions with inherently darker scenes, whereas absorbing aerosols decrease the albedo most strongly over brighter surfaces, with a comparatively lesser impact over darker surfaces (Bellouin et al., 2020; Mishra et al., 2015). On the global average for radiative forcing, absorbing aerosols exert a cooling effect at the top of the atmosphere. In clear-sky maritime scenarios, this radiative forcing is negative. However, when clouds are present in certain regions such as the southeast Atlantic (SEA), the interaction between aerosol and cloud layers can lead to positive radiative forcing, contingent upon the vertical distribution of the aerosols relative to the clouds (Chand et al., 2009; Haywood & Shine, 1997; Keil & Haywood, 2003).

Biomass burning (BB) is the largest source of carbonaceous aerosols globally (Bond et al., 2013; Bowman et al., 2009; Vermote et al., 2009), emitting significant amounts of brown carbon (BrC), light absorbing organic aerosols, and up to 40% black carbon (BC), the strongest light-absorbing aerosol component, into the atmosphere (Andreae & Gelencsér, 2006; Bond et al., 2004; Boucher et al., 2013; Hopkins et al., 2007). The composition of BB aerosols (BBA) is highly variable and often depends on the fuel type and burning conditions, with the less efficient smoldering phase of fires having more organic aerosols (OA) and less BC than the flaming phase (Collier et al., 2016; Jen et al., 2019; Laskin et al., 2015; Levin et al., 2010; Liu et al., 2014; Zhou et al., 2017). BrC exhibits lower mass absorption efficiency compared to BC (Alexander et al., 2008; Jimenez et al., 2009). However, in fires where BrC and BC are co-emitted, the absorption properties of BBA can be influenced by the complex composition which consists of diverse organic compounds capable of oxidation and photochemistry. These reactions, along with particle morphology and the mixing state of the carbonaceous constituents as well as the condensation of gases and other coating materials upon the BC cores ~~as in (Dobracki et al., 2023; Lack & Cappa, 2010)~~ can modify the absorptive characteristics and atmospheric residence time of the aerosols (Dobracki et al., 2023; Feng et al., 2021; Feng et al., 2013; Lack & Cappa, 2010; Saleh et al., 2015). Given the projected global increase in BB events (Jones et al., 2022;

Keywood et al., 2013; Tatro & Zuidema, 2025), an understanding of BBA and their spatial and temporal evolution becomes essential to improve the estimate of their climate forcing.

Southern Africa contributes approximately 35% of the global biomass burning emissions (Granier et al., 2011; Redemann et al., 2021; van der Werf et al., 2010). Annually, between June and October, these emissions are transported westward over the SEA (Holanda et al., 2020) where they overlie a semi-permanent deck of stratocumulus (Sc) cloud (Figure 1) and occasionally mix into the marine boundary layer (MBL) (Zhang & Zuidema, 2021). Consequently, the region is characterized by heavy periodic loadings of BBA, which represent the global maximum of aerosol optical depth (AOD) above clouds (Adebiyi et al., 2015; Waquet et al., 2013).

BBA in this region typically have SSA values ranging between 0.7 and 0.9 from observations (Dubovik et al., 2002; Eck et al., 2013; Haywood et al., 2003). These values generally increase~~, increasing~~ from July to November (Eck et al., 2013), with an average value of 0.85 during the burning season (Dobracki et al., 2023; Eck et al., 2013; Leahy et al., 2007; Pistone et al., 2019), indicating their significant ability to absorb sunlight. BBA also serve as CCN and account for approximately 65% of the total CCN in the Sc cloud deck of the SEA (Andreae & Rosenfeld, 2008; Che et al., 2021; Dedrick et al., 2024; Lenhardt et al., 2023). The warming effect and the ACI by BBA are not well represented in Earth System Models (ESMs), and the SEA region exhibits a large model-to-model divergence of climate forcing due to aerosols (Che et al., 2021; Haywood et al., 2021; Mallet et al., 2020; Sakaeda et al., 2011; Stier et al., 2013). Reliable quantification of the climatic effects of BBA requires an accurate representation of aerosol properties and their vertical and horizontal distributions in models.

Despite recent studies that have documented the transport and characterized the chemical, optical and microphysical properties of the southern African BBA transport (Baars et al., 2021; Denjean et al., 2020a; Denjean et al., 2020b; Dobracki et al., 2023; Holanda et al., 2020; Pistone et al., 2019; Vakkari et al., 2018; Wu et al., 2020), it is still not well understood how the properties of these aerosols evolve during long-range transport. The southern African BBA have been associated with the BC-rich pollution layer above the Amazonian basin following extended transport over the SEA (Holanda et al., 2020). Variations in the chemical composition of BBA at different altitude above the Atlantic have been shown to influence the optical properties of aged BBA (Wu et al., 2020), with low SSA values attributed to the presence of strongly absorbing refractory black carbon (rBC), and minimal contribution from BrC (Denjean et al., 2020b). The mixing state of rBC particles (Denjean et al., 2020b; Sedlacek et al., 2022) as well as the accumulation of a non-absorbing shell by rBC (Redemann et al., 2001) strongly affect the SSA of BBA. Knowledge of the spatial and temporal evolution of BBA, especially during long-range transport is key to understanding the atmospheric processes affecting their lifecycle and their contribution to climate forcing.

While the aging of BBA has recently been parameterized in global climate models (GCMs) (Konovalov et al., 2021; Nascimento et al., 2021), accurately representing the optical and microphysical characteristics of these particles in models remains a challenge due to the intricate chemical and physical processes involved (Brown et al., 2021) and because there have been limited studies on aged BBA. Most research on the evolution and aging of BBA has focused on BBA that has been sampled near the source or in short-term laboratory experiments (Bond et al., 2006; Feng et al., 2021; Kleinman et al., 2020; Liu et al., 2021; Reid et al., 1998; Sedlacek et al., 2022). Due to the lack of observations on longer time scales, there exists a gap in our understanding of how the optical properties of BBA

change during extended transport, such as that over the SEA. Investigating the evolution of aged BBA is, therefore, crucial for improving model capabilities for representing their optical and radiative properties.

The overarching goal of this ~~research~~ study is to examine the evolution of BBA emitted during the annual burning season in southern Africa using remote-sensing observations during their transport across the SEA. Studies on BBA in the region have focused primarily on either continental southern Africa (Abel et al., 2003; Eck et al., 2013; Eck et al., 2003; Queface et al., 2011) or over the ocean (de Graaf et al., 2014; Meyer et al., 2013; Pistone et al., 2019; Redemann et al., 2021; Zuidema et al., 2018). Measurements over the ocean from the ORACLES (ObseRvations of Aerosols above CLouds and their intEractionS) campaign dataset highlighted the connection between BBA composition and absorption, showing a decrease in SSA concurrent with the loss of OA coating on rBC particles, as shown by Sedlacek et al. (2022) and Dobracki et al. (2023). However, our study seeks to expand upon these findings by analyzing aerosol absorption along the entire transport pathway of BBA from the emission source to SEA region (Figure 1). Here, we develop a new methodology that integrates remotely sensed observations from AERONET (AErosol RObotic NETwork) in the BB emission region and 4STAR (Spectrometers for Sky-Scanning, Sun-Tracking Atmospheric Research) over the ocean, collected during the ORACLES campaign. These observations are combined with aerosol age estimates outputs from the WRF-AAM (Weather Research and Forecasting coupled with Aerosol Aware Microphysics module) regional model (Saide et al., 2016) and aerosol properties derived from the WRF-CAM5 (Weather Research and Forecasting coupled with the Community Atmosphere Model version 5). WRF-CAM5 has previously been used to document the chemical composition, hygroscopicity and aerosol-cloud interactions of BBA in the ORACLES campaign region (Howes et al., 2023). This approach enables a comprehensive assessment of the aging of the smoke plume and its impact on optical properties. Particularly, we use the observation of BBA from ORACLES campaign during the burning season of September 2016, August 2017 and October 2018, to investigate the changes in SSA of BBA during their transatlantic transport, spanning the phases of transport over land and, subsequently, over the SEA. Furthermore, using remote sensing to retrieve SSA offers the advantage of sampling aerosols in their ambient state and can be replicated to other domains where AERONET observations are available. ~~The structure of the rest of the paper is as follow: Section 2 provides an overview of the ORACLES field campaign, along with detailed descriptions of the datasets, model configuration, and the methodologies used for data analysis. This includes the separation of marine aerosol contributions in the boundary layer (BL) from total column (TC) retrievals, achieved through the application of a model-derived extinction ratio and aerosol size threshold, with a focus on analyzing BBA in the free troposphere (FT). Section 3 presents the key findings, highlighting the age distribution and variations in the absorptivity of smoke plumes within both the TC and FT, offering insights into the evolution of BBA absorptivity during long-range transport. Section 4 concludes by summarizing the research findings and discussing their broader scientific implications. Supplemental materials provide additional information on instrumentation and data processing, trajectory analyses, aerosol size thresholding used to differentiate between FT and marine boundary layer (MBL) contributions to TC retrievals, and sensitivity results.~~

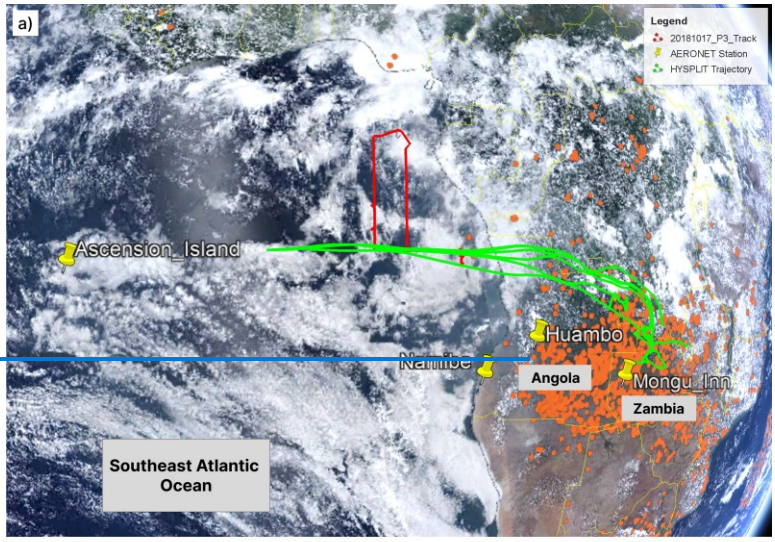
a)
Legend
20181017_P3_Track
AERONET Station
HYSPLIT Trajectory
Ascension_Island
Huambo
Namibe
Angola
Mongu_Inn
Zambia
Southeast Atlantic Ocean

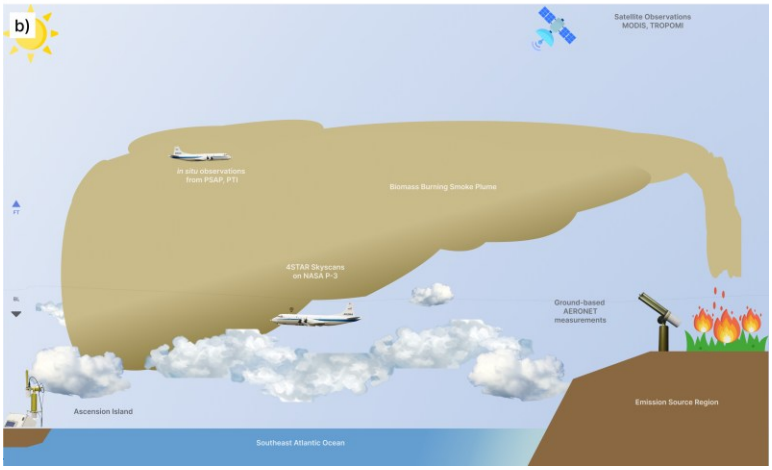
b)
Satellite Observations
MODIS, TROPOMI
in situ observations
from PSAP, PTI
Biomass Burning Smoke Plume
4STAR Skyscans
on NASA P-3
Ground-based
AERONET
measurements
Ascension Island
Emission Source Region
Southeast Atlantic Ocean

190

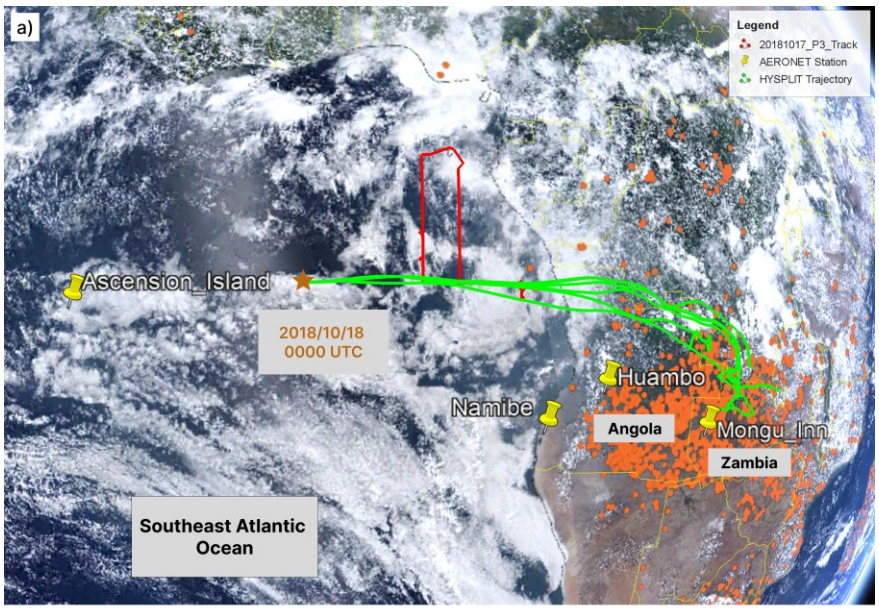

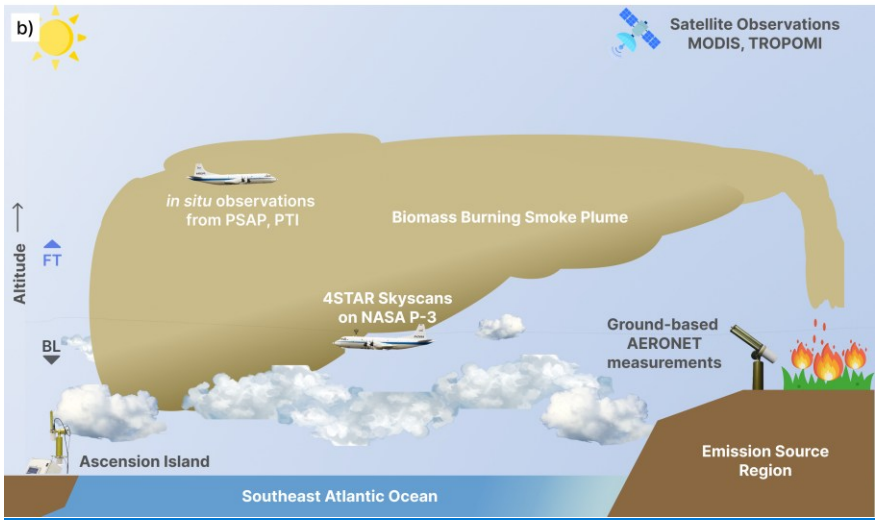

Figure 1:
(a): Satellite image showing the southeast Atlantic Ocean covered by the stratocumulus cloud deck with smoke being advected over it. The smoke from continental fires (orange dots) is being transported, evident by the 7-day backward HYSPLIT trajectory (green) ending between 4000m – 5000m on October 18, 2018, to intersect the P-3 flight (red) on October 17, 2018. ~~from numerous fires (orange dots) in continental southern Africa.~~ Yellow icons represent AERONET

stations selected for this study. while the red line represents the P-3 flight tracks on October 17, 2018, showing the intersection with the smoke transport trajectory.

(https://worldview.earthdata.nasa.gov/, https://www.ready.noaa.gov/HYSPLIT_traj.php, https://earth.google.com, https://aeronet.gsfc.nasa.gov/, https://earth.google.com).

(b): Schematic of the collocation of observations in the southeast Atlantic region during the ORACLES mission. Satellite observation from Moderate Resolution Imaging Spectroradiometer (MODIS) and TROPOspheric Monitoring Instrument (TROPOMI). Airborne observations from 4STAR, ground-based observations from AERONET, in- situ measurement from Particle Soot Absorption Photometer (PSAP) and Photo-Thermal Interferometric (PTI) Particle Absorption Monitor. Measurements from 4STAR and AERONET are presented in this study.

2 Data and methods

2.1 NASA ORACLES campaign

A comprehensive overview of the ORACLES campaign is presented by Redemann et al. (2021); Here, we summarize the methods and data analysis techniques that are relevant to this study. The campaign provided process-level understanding of aerosol effects in the SEA that can be applied in the parameterization of ACI and ARI in ESMs (Redemann et al., 2021). The campaign overlapped with other field experiments (Zuidema et al., 2016) – CLARIFY-2017: Cloud-Aerosol-Radiation Interactions and Forcing for Year 2017 (Haywood et al., 2021), LASIC: Layered Atlantic Smoke Interactions with Clouds (Zuidema et al., 2018), AEROCLO-sA: AErosols, RadiatiOn and CLOuds in southern Africa (Formenti et al., 2019) – in a synergistic effort to determine the influence of southern African BBA on cloud properties and the energy balance in the SEA region. The ORACLES campaign occurred between 2016 and 2018 with field deployments in Walvis Bay, Namibia (September 2016), and in São Tomé and Principe (August 2017, and October 2018). The NASA P3-B aircraft was home to a suite of in-situ and remote-sensing instruments including the 4STAR (Dunagan et al., 2013) and the ER-2 (a high-altitude aircraft) was home to a suite of additional remote sensing instruments. A total of 56 research flights:12 from the ER-2, only in 2016, and 44 from the P-3B across the three deployments, shown in Figure 2, with over 450 science flight hours, collected data on aerosol optical properties (Pistone et al., 2019; Redemann et al., 2021). This study uses 4STAR retrievals of BBA properties (Table 1) from all three campaign deployments made on the P-3B aircraft, to study the evolution of light absorption properties of BBA.

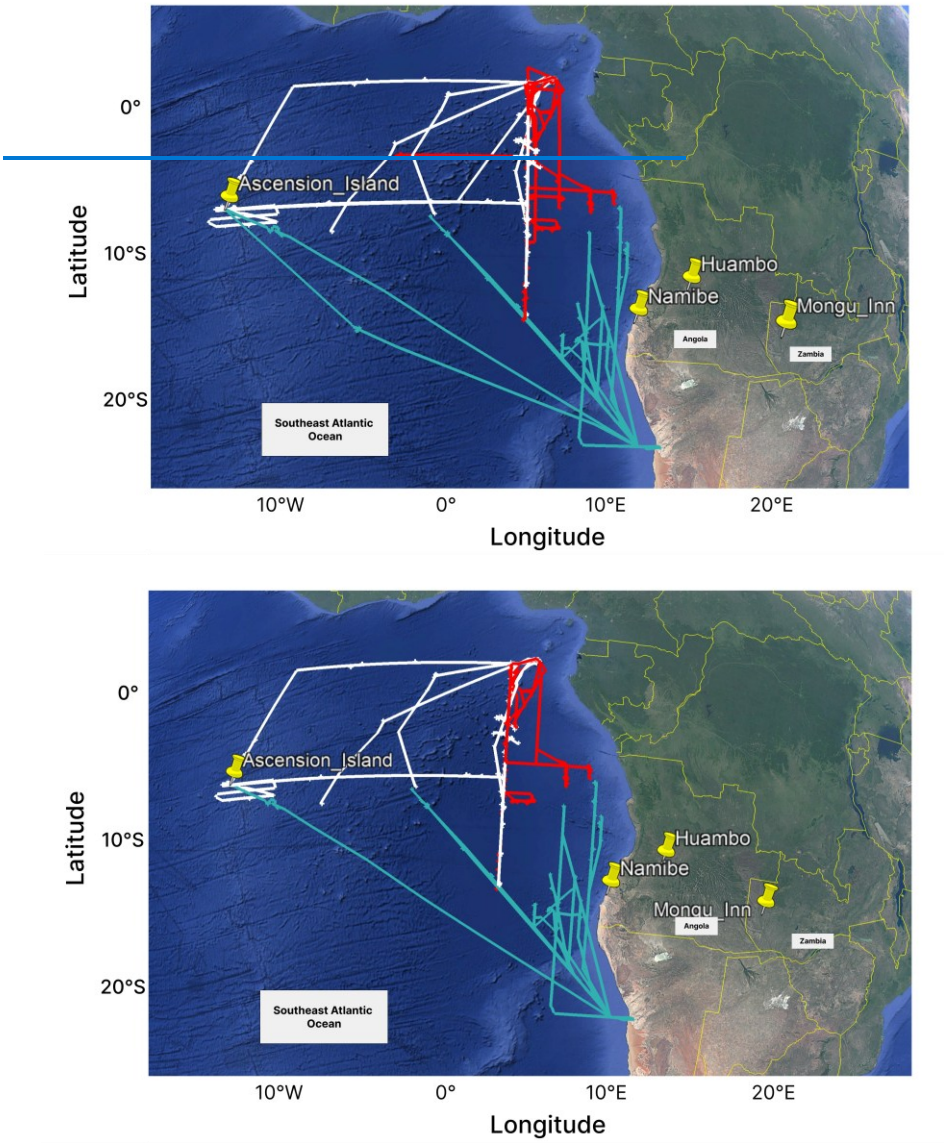

Figure 2: Map of the SEA showing the NASA P-3B flight tracks during ORACLES 2016 (cyan), 2017 (white) and 2018 (red) for observation days analyzed in this study. The ORACLES aircraft deployed out of Walvis Bay, Namibia in 2016 and São Tomé and Príncipe in 2017 and 2018. Regional AERONET stations are identified using yellow icons. Background imagery from Google Earth (https://earth.google.com) - Data SIO, NOAA, U.S. Navy, NGA, GEBCO, Image Landsat / Copernicus.

~~A map of the SEA showing flight tracks of the NASA P-3B aircraft during ORACLES 2016 (cyan), 2017 (white) and 2018 (red). The ORACLES team deployed out of Walvis Bay, Namibia in 2016 and São Tomé and Príncipe in 2017 and 2018. In this study, we focus on 2016 and 2017 observations. Regional AERONET stations are identified using yellow icons.~~

2.2 Ground-based measurements

AERONET, a global sun photometer network, provides long-term, continuous measurement of AOD and retrievals of aerosol microphysical, optical, and radiative properties for aerosol characterization and validation of satellite retrievals (Holben et al., 1998). In this study, we used AERONET Version 3 inversion products (Table 1) from both almucantar (ALM) and hybrid scans including cloud-screened (level 1.5) and quality assured (level 2.0) data (Giles et al., 2019; Sinyuk et al., 2020) from four AERONET stations: three situated in continental southern Africa, **Mongu Inn (Zambia), Huambo (Angola), Namibe (Angola)**; and one in the maritime SEA - **Ascension Island (United Kingdom Territory)** (Table 2). These stations were carefully selected based on their geographic locations aligning with the trajectory of BBA from continental Africa and over the ocean, as shown in Figure 1. Specifically, column-integrated measurements of AOD, SSA, and extinction Ångstrom exponent (~~hereafter~~ EAE) for September 2016, August 2017, and October 2018 were used, coinciding with the observation periods of ORACLES 2016, 2017, and 2018. The Namibe site was inactive during the ORACLES 2018 campaign, providing data only for 2016 and 2017, while the Huambo site, established in 2017, contributed observations for both 2017 and 2018. At Ascension Island and Namibe, fewer observations were available due to the increased cloud cover along the coast and over the SEA. Therefore, to ensure an adequate sample size at Ascension Island and Namibe, we included level 1.5 data in our analysis when level 2.0 data was unavailable. More information about the AERONET stations utilized in this study is provided in Table 2.

Table 1: Summary of observation data products and aerosol properties used in this study.

Data	Product	Properties	Data Access
AERONET	Inversion (level 1.5, 2.0) product version 3: All Observation	Aerosol Optical Depth (AOD) & Single Scattering Albedo (SSA) *440, 675, 870 nm* Extinction Ångstrom Exponent (EAE) *440-870 nm*	https://aeronet.gsfc.nasa.gov/
4STAR	4STAR-aeroinv_P3	Aerosol Optical Depth (AOD) & Single Scattering Albedo (SSA) *500, 675, 870, 975 nm* Extinction Ångstrom Exponent (EAE) *500-975 nm*	https://espoarchive.nasa.gov/archive/browse/oracles/P3/4STAR-aeroinv

2.3 Airborne measurements

4STAR was integrated on the NASA P-3B aircraft to measure direct solar beam and sky radiances (Dunagan et al., 2013), collecting data in three modes: a sun-tracking mode (LeBlanc et al., 2020; Segal-Rosenheimer et al., 2014); a sky-scanning mode (Pistone et al., 2019); and a zenith mode (LeBlanc et al., 2015). 4STAR is unique in its ability to perform AERONET-like measurements from an aircraft, making it suitable for studying remote regions that AERONET does not cover. It also frequently offers a more comprehensive observational dataset through its deployment alongside in-situ instrumentation, as in the ORACLES campaign. This study primarily examines observations made in the sky-scanning mode, in which, analogous to AERONET, the 4STAR instrument performs ALM scanning to measure the angular distribution of brightness in the sky. In addition, retrievals from principal plane (PPL) scans are also used, as ORACLES flights largely occurred near solar noon, limiting the angular range of ALM scans. As such, we selectively considered both ALM and PPL scans if they met specific quality control (QC) criteria. Here, we processed 4STAR sky scans using the QC criteria from Mitchell et al. (2023). These criteria were adapted from Pistone et al. (2019) for four-wavelength 4STAR retrieval of ORACLES 2016-2018 and serve as a proxy for AERONET level 1.5 aerosol inversion standards. The criteria are: (1) AOD (400 nm) > 0.2, (2) altitude difference < 50 m, (3) sky error < 10%, (4) minimum scattering angle < 6°, (5) maximum scattering angle > 50°, (6) mean scattering angle difference < 3° (between 3.5 and 30°), (7) maximum scattering angle difference < 10° (between 3.5 and 30°), (8) roll standard deviation < 3°, (9) passes retrieval boundary test - ensuring that the retrieval is within limits of parameter space, and (10) maximum altitude < 3000 m. A summary of the valid QC'd 4STAR retrievals of SSA, AOD, EAE (Mitchell et al., 2023) used from the ORACLES dataset (ORACLES, 2020) for all three deployments is given in Table 1.

Table 2: Site information and total observation count for AERONET and 4STAR.

Site Name	Latitude	Longitude	Elevation (m)	Number of Observations *(2016, 2017, 2018)*
Ascension Island	-7.97	-14.41	30	77 *(17, 53, 7)*
Namibe	-15.15	12.17	11	135 *(71, 64, -)*
Huambo	-12.86	15.7	1670	342 *(-, 250, 92)*
Mongu Inn	-15.26	23.13	1040	444 *(126, 167, 151)*
4STAR	-	-	-	308 *(77, 139, 92)*

2.4 WRF-CAM5: Concept and Configuration

WRF-CAM5 is an adaptation of WRF-Chemistry (WRF-Chem) model (Grell et al., 2005), which integrates the physics and aerosol packages of the global CAM5 (Ma et al., 2014; Zhang et al., 2015a), making it suitable for studying multi-scale atmospheric processes and evaluating aerosol and physics parameterizations in global climate models

(Wang et al., 2018). WRF-CAM5 has been widely applied to investigate air quality and climate interactions in Asia and the United States (Campbell et al., 2017; Wang et al., 2018; Zhang et al., 2015b)

The WRF-CAM5 model incorporates advanced cloud schemes, including the two-moment cloud microphysics scheme (Morrison & Gettelman, 2008), the shallow cumulus scheme of Bretherton and Park (2009), turbulence parameterization (Bretherton & Park, 2009), the Zhang-MacFarlane convective cloud scheme (Zhang & McFarlane, 1995), and aerosol-cloud feedback mechanisms (Lim et al., 2014; Song & Zhang, 2011). It also includes a mixed-phase and ice clouds parameterization (Niemand et al., 2012), a modal aerosol module (MAM3) (Liu et al., 2012), coupled with a gas-phase chemistry scheme (Zaveri & Peters, 1999), enabling the determination of aerosol (including smoke) properties. Aerosol optical properties are calculated using WRF-Chem routines (Fast et al., 2006) with Mie theory calculations, and cloud droplet activation based on the Fountoukis and Nenes (2005) and Zhang et al. (2015a) scheme, considering the activation of giant CCN and insoluble particles, such as dust and black carbon. The refractive indices for organic aerosols (1.45+0i) and black carbon (1.85+0.71i) were assumed to be constant across the shortwave radiation spectrum (Shinozuka et al., 2020a).

Recent studies have demonstrated the model's accuracy in capturing smoke concentration, aerosol properties, and the vertical distribution of BBA in the SEA region (Chang et al., 2023; Doherty et al., 2022). In this study, WRF-CAM5 was configured with a horizontal resolution of 36 km and 74 vertical layers across the spatial domain 41°S-14°N, 34°W-51°E, initialized every five days using the National Center for Environmental Prediction (NCEP) Final Operational Global Analysis (NCEP FNL) and Copernicus Atmosphere Monitoring Service (CAMS) reanalysis datasets as detailed in Shinozuka et al. (2020a) and Doherty et al. (2022), with daily smoke emissions from the Quick-Fire Emissions Dataset version 2 (QFED2) (Darmenov & da Silva, 2015).

2.5 Plume Age Derivation

To estimate the age of the aerosols, defined as the time since emission, we utilized carbon monoxide (CO) tracers coupled with smoke emissions within the WRF-AAM model. The WRF-AAM model, which share similar configurations with WRF-CAM5, allows for region- and case-specific microphysical parameterization of aerosol-cloud interactions (Thompson & Eidhammer, 2014) and aerosol-radiation interactions (Saide et al., 2016), thus facilitating the characterization of aerosol aging processes.

The regional model was set up with a horizontal resolution of 12 km, encompassing the geographical area (41°S-14°N, 34°W-51°E). This domain size is considered sufficiently extensive to contain nearly all fires across the African continent (Howes et al., 2023; Saide et al., 2016). The fire emission source for the model is based on QFED2 which uses fire radiative power (FRP) as a proxy for estimating fire emissions. QFED2 leverages the cloud correction techniques developed in the Global Fire Assimilation System (GFAS) to refine emission estimates (Darmenov & da Silva, 2015). Location and FRP of fires are sourced from MODIS Level 2 fire products (MOD14 and MYD14), coupled with MODIS Geolocation products (MOD03 and MYD03). The NCEP Global Forecasting System (GFS) meteorology serves as the primary driver for the WRF-AAM model which incorporates daily smoke emissions from

QFED2, which are subsequently adjusted to correspond with satellite-derived AOD using a near real-time inversion algorithm, as detailed in Saide et al. (2016).

The model was run in a forecast mode to estimate the time since smoke emission, with a maximum aerosol age of 14 days. The model attaches age tracers to the CO released at BB emission sites. These tracers, which are treated as chemically inert gases, are tagged for each day, and tracked for up to two weeks, allowing sufficient time for the smoke to travel across the SEA. This model setup operates in a cycle, where each day, the tracers from the previous day are shifted to the next older tracer bin, continuing until they reach the 14-day mark. At this point, they accumulate in the oldest bin. The age of the smoke plume is determined by averaging the concentration of these tracers at any given location. However, this setup has limited accuracy at the upper end of the age estimate; for instance, smoke older than 14 days is still averaged as 14 days old, even if it contains an equally concentrated mixture of tracers that have been out for different lengths of time beyond the 14-day tracking period. In comparison, the HYSPLIT model (Stein et al., 2015), also driven by the NCEP GFS meteorology, typically yields age estimates that are approximately one day lower than the WRF-AAM. Given that HYSPLIT employs a simpler scheme at coarser resolutions, it is likely that the age estimates from WRF-AAM model are more accurate and reliable. The plume ages assigned within a given column exhibited minimal variability (see supplemental information S6), which gives confidence to the method.

To determine the effective aerosol age for AERONET and 4STAR observations, which are columnar, the WRF-AAM model's assigned plume age in the vertical layers above these instruments is weighted by their respective extinction coefficients (β_ext) per equation (1):

$$Aerosol\ age = \frac{\int_{s_{elv}}^{toa} \beta_{ext*}\ \text{plume age}\ dz}{\int_{s_{elv}}^{toa} \beta_{ext}\ dz}, \quad (1)$$

Where s_{elv} is the elevation of the AERONET station or the flight altitude of observation for 4STAR and toa is the top of the atmosphere.

2.6 Spatiotemporal Collocation and Analysis

The AERONET inversion products provide AOD and SSA at four wavelengths: 440, 675, 870, and 1020 nm. The relationship between AOD and wavelength, defined by the Ångström exponent formula (Eck et al., 1999) is used to compute EAE(α):

$$EAE(\alpha) = -\frac{\ln(\tau_1) - \ln(\tau_2)}{\ln(\lambda_1) - \ln(\lambda_2)}, \quad (2)$$

Where τ_1 and τ_2 are AOD at wavelengths λ_1 and λ_2. In AERONET and 4STAR retrievals, EAE(α) is calculated from AOD measurements at 440 nm and 870 nm.

Given the differences in the temporal resolution of 4STAR and AERONET observations and the WRF-AAM model outputs, we adapted the model output to match all AERONET and 4STAR observations spatially and temporally, to yield the extinction-weighted aerosol age calculated using extinction at 532 nm as in Equation (1). However, since

AERONET does not provide retrievals at 532 nm, we computed the equivalent AOD and SSA at 532 nm to correspond with the model's output using the Ångström formula (equation 2) for AOD, and the linear interpolation equation for SSA.

2.7 Separating Boundary Layer (BL) contributions from Total Column (TC) observations

In the SEA, as ocean surface temperatures rise, the BL deepens and decouples, with the BL height (BLH) increasing away from the African coast, from approximately 1300m to 1700m, before transitioning to a cumulus-dominated cloud regime, as explained ~~The BL, the atmospheric region adjacent to the Earth's surface, is characterized by persistent small-scale turbulence driven by wind shear and thermal convection, and is strongly influenced by surface conditions (Deardorff, 1972; Seidel et al., 2010). In the SEA, as ocean surface temperatures rise, the BL deepens and decouples, with stratocumulus clouds frequently observed in the upper part of the decoupled BL. Away from the African coast, the BL height (BLH) increases from approximately 1300m to 1700m, before transitioning to a cumulus-dominated cloud regime, as explained~~ by Zhang and Zuidema (2019, 2021) and Ryoo et al. (2021). Over land, BBA dominate the deep BL, extending beyond 6 km and are then advected over the SEA above the cloud layer by free troposphere (FT) winds ~~Over the continent, BBA dominate the deep BL, extending beyond 6 km and are advected over the SEA, by the FT winds~~ (Ryoo et al., 2021), particularly from August to October during strong south African Easterly Jet (AEJ-S) episodes ~~where they reside above the cloud layer. This transport is most pronounced from August to October, coinciding with the strongest episodes of the south African Easterly Jet (AEJ-S)~~ (Adebiyi & Zuidema, 2016). The radiative effects of aerosols in the SEA region are heavily influenced by the interplay between the aerosol layer and cloud layer ~~The radiative effects of aerosols in the SEA region are heavily influenced by the interplay between the aerosol layer and cloud layer~~ (Chang & Christopher, 2017; Zhang & Zuidema, 2021).

While BBA generally maintain their path within the FT over the SEA, large scale subsidence (Wilcox, 2010) and the low-level easterlies (Diamond et al., 2018) ~~occasionally~~ can bring the aerosol layer int~~r~~o contact with the BL clouds, particularly between June and August, causing the entrainment of aerosols and altering their properties (Dobracki et al., 2025) ~~Dobracki et al. (2025) (Dobracki et al., 2024)~~. Marine aerosols, particularly sea salt aerosols, have higher SSA values and enhanced CCN activity, which are altered when they mix with foreign particles especially in coastal regions near anthropogenic sources (Adachi & Buseck, 2015; Pósfai et al., 1995). Dang et al. (2022) showed that BBA sampled during ORACLES dominate the FT while sea salt aerosols dominate the BL over the SEA with a fraction of BBA mixed with sea salt aerosols in the BL. Therefore, our goal of investigating the evolution of BBA from TC observations is complicated by the potential contribution of non-BBA aerosols from the MBL. To address this, and given that AERONET and 4STAR provide columnar retrievals above the observation altitude, we employed a two-pronged approach, detailed in Section 2.7.1 and 2.7.2, to isolate the FT aerosol from the columnar observations. First, we applied a model-derived ratio to partition aerosol loading in the FT and BL over the SEA. Subsequently, we implemented a size thresholding technique to exclude contributions from larger particles, ensuring our analysis remains focused on BBA properties.

2.7.1 Application of model-derived extinction ratio

To address the potential influence of MBL aerosol properties on the TC observations by AERONET and 4STAR over the SEA, we use a model-derived vertical distribution of extinction to estimate the FT contributions to the TC measurements, while assuming an external mixing state of particles over the ocean. Specifically, we applied model-derived ratios of extinction in the BL relative to the TC (R_{BL}), and in the FT relative to the TC (R_{FT}) to:

(i) all AERONET observation at Ascension Island and Namibe;
(ii) 4STAR observations when the NASA P-3 aircraft was flying within the BL.

To compute R_{BL} (equation 3) and R_{FT}, we applied BLH values from WRF-CAM5 for both sets of observations. The BLH values are estimated according to (Chang et al., 2023) and validated with radiosonde observations at Ascension Island (Zhang & Zuidema, 2019).

$$R_{BL} = \frac{\int_{s_{elv}}^{BLH} \beta_{ext} dz}{\int_{s_{elv}}^{toa} \beta_{ext} dz}, \quad (3)$$

$$R_{FT} = 1 - R_{BL}, \quad (4)$$

Using the computed ratios, we partitioned the columnar AOD (AOD_{TC}) measurements at locations (i) and (ii)using the following equations:

$$AOD_{BL} = R_{BL} * AOD_{TC}, \quad (5)$$

$$AOD_{FT} = R_{FT} * AOD_{TC}, \quad (6)$$

Here, AOD_{BL} and AOD_{FT} represent the partial AOD at 532 nm within the BL and FT, respectively. For (i), AOD_{TC} refers to the columnar AOD above the site's elevation and AOD_{BL} represents the portion of AOD between that elevation and the BLH. For (ii), AOD_{TC} refers to the columnar AOD above the P-3 aircraft altitude, while AOD_{BL} represents the portion of AOD between the P-3 flight altitude and the BLH.

We next calculated the proportion of aerosol age and SSA within the FT using the following:

$$Aerosol_{age_{FT}} = \frac{\int_{BLH}^{toa} \beta_{ext} * \text{plume age } dz}{\int_{BLH}^{toa} \beta_{ext}\, dz}, \quad (7)$$

$$SSA_{FT} = \frac{(SSA_{TC} * AOD_{TC}) - (SSA_{BL} * AOD_{BL})}{AOD_{FT}}, \quad (8)$$

While the WRF-CAM5 BLH values generally agree with observational data, our analysis indicates that the model significantly underestimates aerosol loading in the BL, a limitation also highlighted in prior studies (Figure 8-11, Doherty et al. (2022)). Despite having the most accurate model representation of aerosol properties in the SEA region (Doherty et al., 2022), this underestimation in the BL by WRF-CAM5 (see supplemental Figures S7 – S9) affects the representation of BBA properties in the FT at location (i) and (ii) , with physically unrealistic values. To address this, we applied an assumed SSA_{BL} value of 1, recognizing that this introduces a source of uncertainty to the analysis, as it

assumes that all aerosols in the BL are purely scattering and does not account for the occasional mixing of BBA with marine sea salt in the BL. To aid the separation of BL and FT BBA, we applied an EAE screening, described below.

2.7.2 Application of Extinction Ångstrom Exponent (EAE) Thresholds

The extinction Ångstrom Exponent (EAE) is sensitive to the size distribution of aerosol particles (Aladodo et al., 2022; Eck et al., 1999; Schuster et al., 2006). Fine-mode aerosol particles, such as smoke typically have a higher EAE (usually > 1) than coarse-mode aerosols such as marine sea salt, which typically have a lower EAE (< 1). Along with implementing the model-derived extinction ratio outlined in Section 2.7.1, to further discard contributions of other aerosols to the columnar measurements, particularly in atmospheric layers above location (i) and (ii), we applied an EAE filter. We posit that EAE values < 1 would indicate the presence of sea salt aerosol whereas EAE values ≥ 1.5 would indicate the dominance of BBA (Eck et al., 1999) while layers with measured EAE values between 1 and 1.5 contain varying degrees of sea salt and BBA following the results of Dang et al. (2022). We tested four EAE threshold values: ≥ 0.75, ≥ 1, ≥ 1.2, and ≥ 1.4, to successively exclude such measurements, retaining only fine particles while carefully considering the data processing. Our analysis of the EAE thresholding (see supplemental information S3 for more details) suggests that EAE of 1.5 for BBA might be applicable near emission sources, lower values during transport and aging led us to choose a lower threshold of 1.2 to have more robust statistics over the ocean.

3 Results and Discussion

3.1 Age distribution of smoke plumes

The aerosol age (a) and extinction (b) on October 17, 2018, as derived by the WRF-AAM model is shown in Figure 3, with the altitude track of the P-3 aircraft, which flew over the SEA between 7:00 – 15:00 UTC (see also supplemental Figure S10), overlaid onto the curtain plot. For this case, the model simulates particles at altitudes below 2 km and above 8 km to be substantially older, with plume age ranging from 9 – 12 days, than those in the mid FT (3 – 7 km) with age ranging from 3 – 8 days. The age of the plume sampled between 12:00 – 13:00 UTC at the flight intersection with the HYSPLIT trajectory shown in Fig. 1 ranged from 4 – 8 days, relative to HYSPLIT age range of 4 – 6 days (see supplemental Figure – S1). In Figure 3(b), the vertical distribution of aerosol extinction generally revealed maximum extinction within the lowest 2km. The model demonstrated a consistent inverse relationship between extinction and height, with extinction decreasing as height increased, reaching a minimum above 6 km ~~In Figure 3(b), the vertical distribution of aerosol extinction revealed maximum extinction below 1 km. The model demonstrated a consistent inverse relationship between extinction and height, with extinction decreasing as height increased, reaching a minimum above 6 km~~.

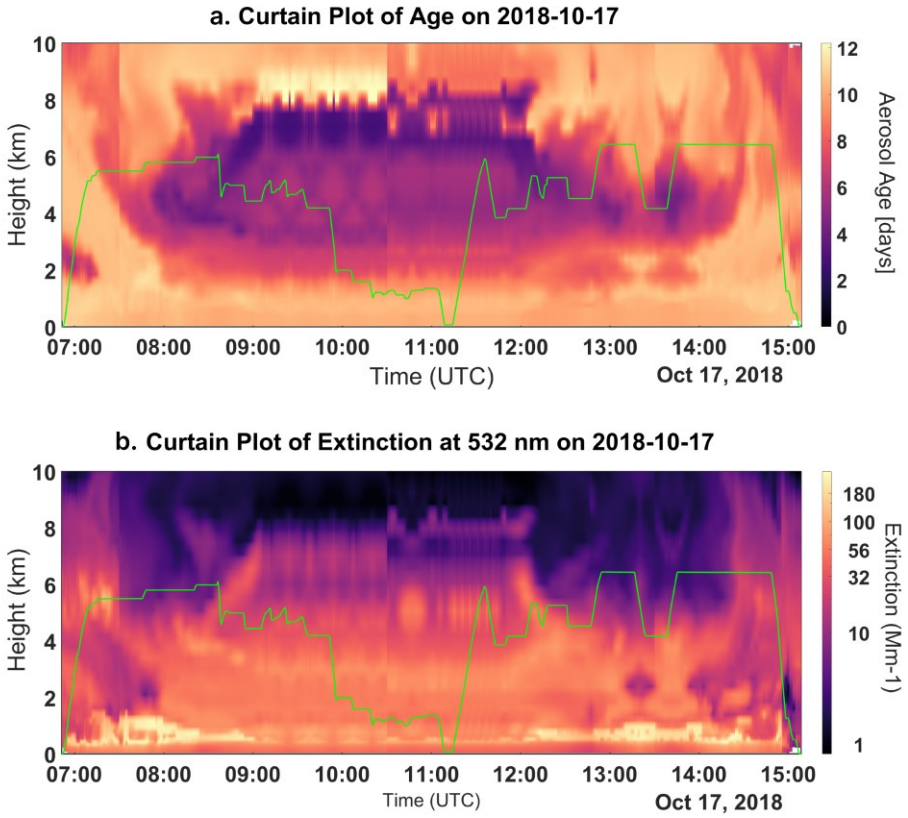

Figure 3: WRF-AAM curtain plot with altitude on the Y-axis and time in UTC on the X-axis, showing the smoke plume age forecast (a) and aerosol extinction (b) along the P-3 track (solid green line) during research flight 10 of the third ORACLES deployment on October 17, 2018. The smoke plume age is calculated as the average of the tracer concentration in each age bin.

The ~~modelled~~ modeled vertical distribution of aerosol age and extinction across all ORACLES flight missions and exemplified in Fig. 3 reveals a distinct pattern: aerosols around 7km, within a central altitude band of 3 – 8 km, are younger and likely represent aerosols recently transported by the FT jet. In contrast, aerosols below 1 km and above 8 km over the ocean appear to have an older connection to their source regions, suggesting they either followed a different transport route than the FT aerosols or were recirculated by the AEJ-S, as previously described by Adebiyi and Zuidema (2016).

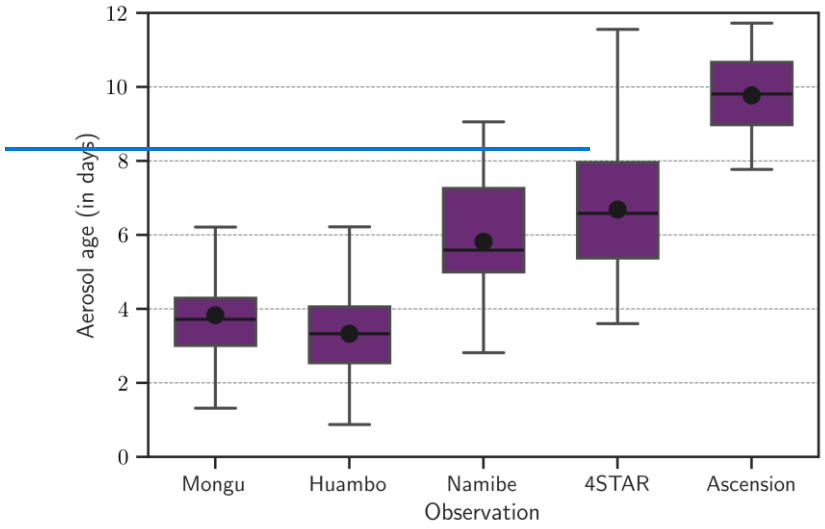

~~Figure 4: Box-whisker plots of the extinction-weighted aerosol age for available observation at each site. The boxes represent the 25th (lower box) and 75th (upper box) percentile while the whiskers show the 10th (lower whisker) and 90th (upper whisker) percentiles of aerosol age. The black circle represents the mean aerosol age while the solid line across the box represents the median. Data plotted represents the columnar measurements across all observations.~~

The distribution of ~~summary statistics of~~ aerosol age from all AERONET and 4STAR observations considered in this study (Fig. 4) show the oldest BBA are observed near Ascension Island (7.9°S, 14.4°W), a remote island about 2000 km away from the African coast. WRF-AAM outputs predict the samples at Ascension Island to be aged between approximately 7 – 12 days, with a mean age of approximately 10 days, while for 4STAR observations, WRF-AAM show that the aerosol age ranged between 3 and 12 days, with a mean age of about 7 days. However, younger BBA were observed over land, closer to the source region of the fires. The plumes sampled at Mongu, Huambo, and Namibe, were aged between 1 – 7 days, 0 – 6 days, and 3 – 9 days, respectively, with mean age of approximately 4, 3.5, and 6 days. The youngest aerosols in the source region were sampled at Huambo (12.8°S, 15.7°E) and Mongu (15.2°S, 23.1°E), with over 75% of all observations at both stations aged less than 4 days. The mean age of aerosols near the African coast was approximately 6 days, suggesting that the smoke measured at Namibe (15.15°S, 12.17°E) has migrated from the primary burning region at Mongu and Huambo. This is further supported by trajectory analysis (see supplemental Figure S1) and by the limited count of active fires recorded in the vicinity of Namibe during the campaign period as shown in Fig. 1. 4STAR observations show a wider age range than those from AERONET sites. This variability is likely attributed to the ORACLES flight strategy, which sometimes targeted freshly emitted smoke from new fires, resulting in the lower age range of 3 to 6 days. The ~~modelled~~ modeled aging pattern suggests the smoke originating from the continent follows a relatively steady trajectory up to Ascension Island. This is supported by HYSPLIT trajectory analysis (see supplementary information – S2), which reveals that the

majority of air masses from the burning region follow a similar path westward, typically reaching Ascension Island within 10 to 12 days.

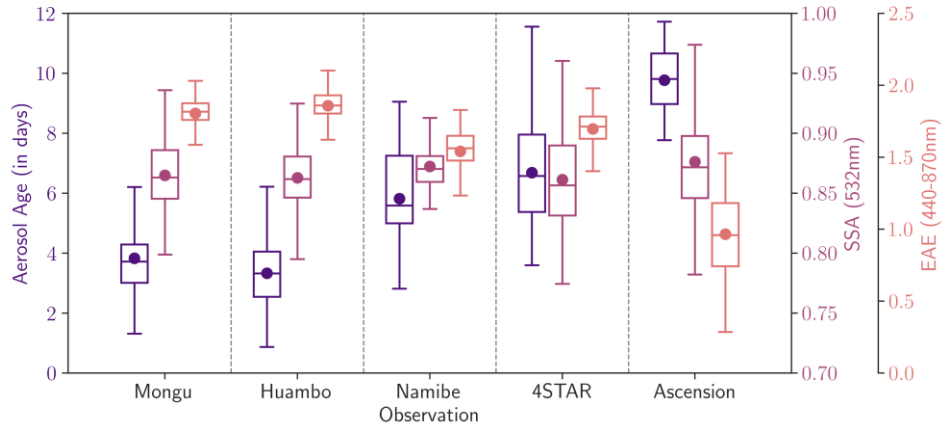

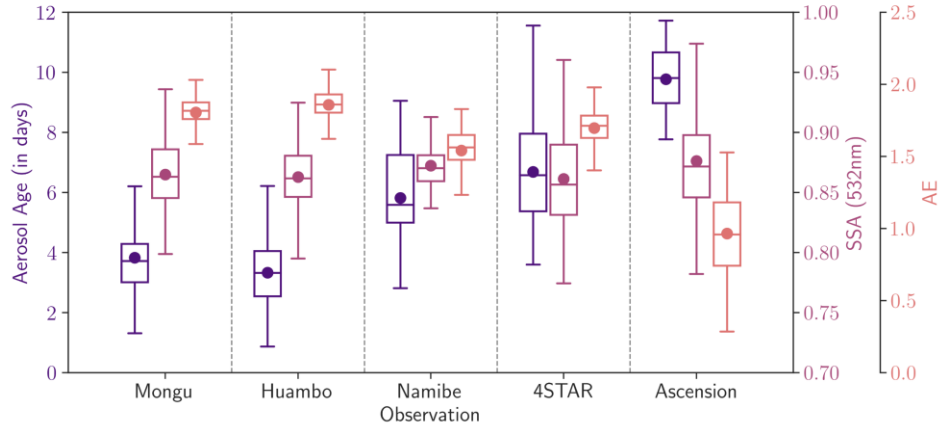

Figure 46: Box and whisker plots showing the distribution of aerosol age (violet), SSA_{532nm} (magenta) and EAE (peach) in the TC for available observation at each site. The box-whisker plot shows the 10th (lower whisker), 25th (lower box), 50th (median), 75th (upper box), and 90th (upper whisker) percentiles. The mean value for each parameter is marked with the circle.

Formatted: Indent: First line: 0"

Formatted: Indent: First line: 0"

3.2 Changes in total column SSA with age

Next, we investigate the relationship between SSA and the model-derived age, stratified by the EAE in the TC over the entire study region. We do this by combining ~~integrating~~ the available collocated AERONET, 4STAR and WRF-AAM output datasets from September 2016, August 2017, and October 2018. Combining data from all

three months together provides additional dynamic of change in SSA with time through the burning season months as shown in Eck et al. (2013). The distribution of SSA and EAE by observation site is shown in Fig. 4, while Figure 5 shows SSA at 532 nm and EAE as a function of model-derived aerosol age for all observations in the TC. ~~Their distribution by observation site is shown in Fig. 6.~~ The cluster of high-EAE data, seen between 0 to 4 days in Fig. 5, is primarily made up of measurements in the burning region from Mongu and Huambo, with average EAE values of 1.81 and 1.86, respectively (Fig. 46), indicating a dominance of BBA in the TC at these locations. Correspondingly, the TC SSA ranges between 0.77 and 0.97, with mean TC SSA of 0.86 at the two locations, with over 75% of the data below 0.90.

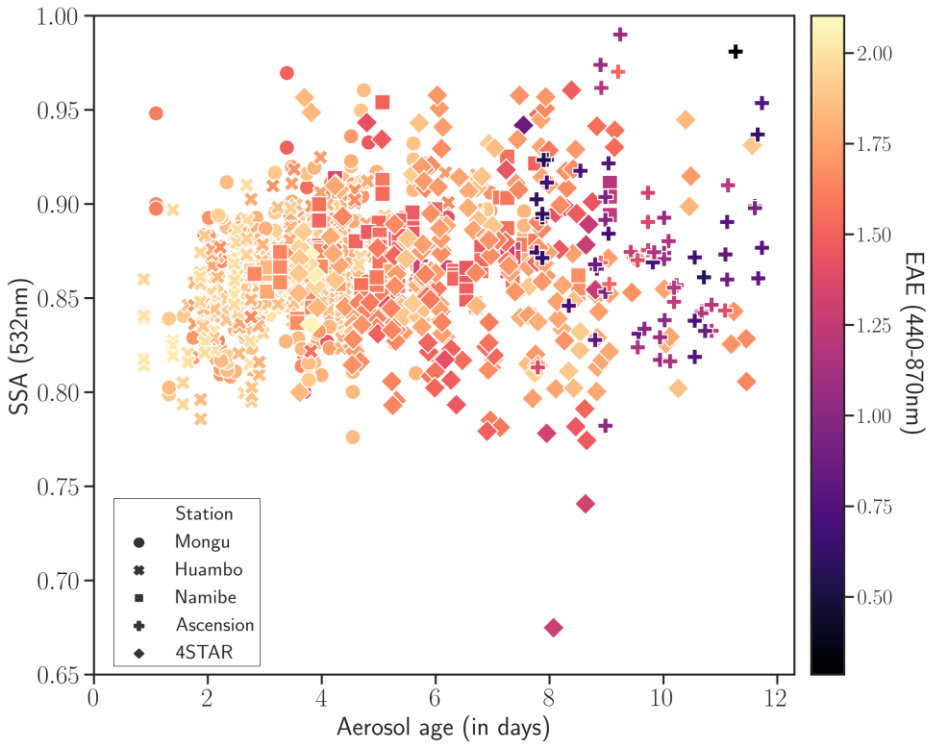

Formatted: Indent: First line: 0"

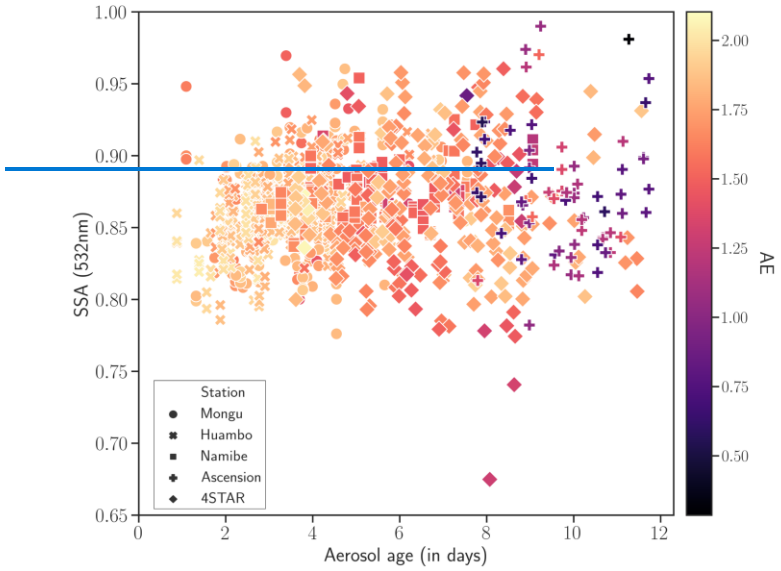

Figure 5: Relationship between SSA_{532nm} (y-axis), EAE (color bar), and aerosol age (x-axis) in the total atmospheric column (TC). ~~The different markers represent the site of observation while the marker shading~~ represents the EAE.

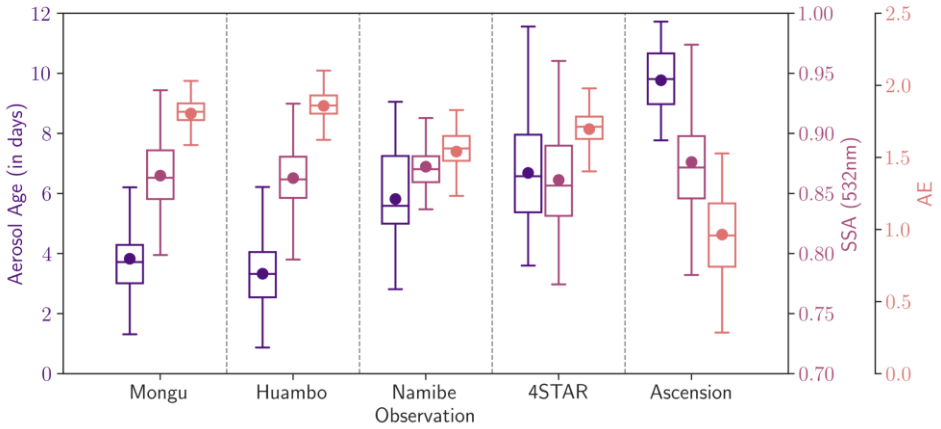

~~**Figure 6: Box-and-whisker plots showing the distribution of aerosol age (violet), SSA_{532nm} (magenta) and AE (peach) in the TC for available observation at each site. The box-whisker plot shows the 10th (lower whisker), 25th (lower box), 50th (median), 75th (upper box), and 90th (upper whisker) percentiles. The mean value for each parameter is marked with the circle.**~~

The TC SSA result in the source region at Mongu and Huambo implies that fresh BBA (≤ 4 days) is optically dark and highly absorbing of solar radiation as indicated by low SSA values (Table 4), which is consistent with previous

findings (Abel et al., 2003; Eck et al., 2013; Haywood et al., 2003; Leahy et al., 2007) in the region. A decrease in TC EAE is observed with increasing distance from the source region (see supplemental Figure S14), indicating larger particle sizes at more remote locations over the SEA. At Namibe, the mean TC EAE is 1.54, with a mean TC SSA of 0.87, ranging from 0.83 to 0.95. This observed trend of increasing particles size align with in-situ aerosol size measurements (Howes et al., 2023). Aerosols over the SEA exhibit a broad range of TC EAE values, from 0.28 and 2.0, reflecting significant heterogeneity in particle sizes within the TC. These observations have a mean TC SSA of 0.86 for 4STAR, with a range between 0.67 – 0.96, and a mean TC SSA of 0.87 at Ascension Island, ranging from 0.78 to 0.99. Some retrievals over the SEA showed both low SSA values (< 0.8) and low EAE values (≤ 1.0), suggesting the possible presence of other aerosol types at Ascension Island (Howes et al., 2023), or a combination of coarse non-or less-absorbing particles and BBA within the same column.

Upon applying an EAE threshold of 1.2 to the TC, we binned the aerosol age into two-day intervals and estimated the mean TC SSA for each bin (Fig. 67). The result shows that mean TC SSA increases with age, changing from 0.84 within 0 to 2 days of emission over land in the source region up to 0.87 after 6 to 8 days, then decreases over the ocean, reaching approximately 0.86 after 10 to12 days. This result indicates changes in aerosol optical properties during different stages of transport.

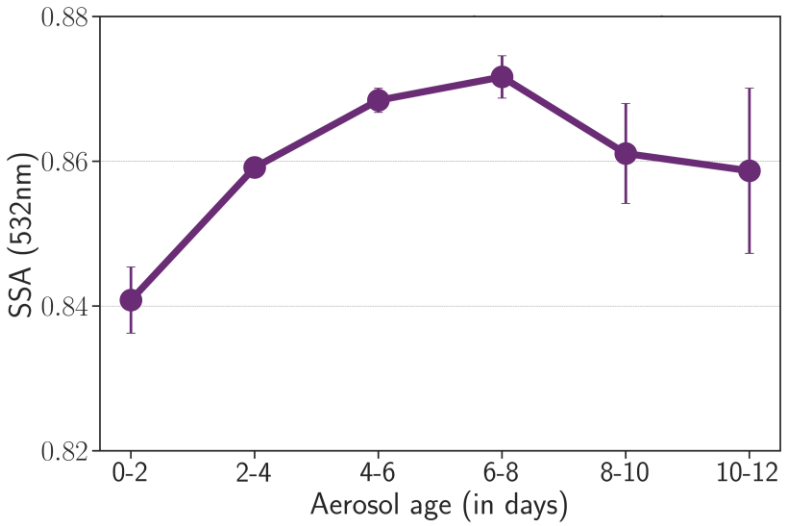

Figure 67: Mean SSA (at 532 nm) within the vertical column (TC SSA) as a function of aerosol age for the optimal threshold (EAE ≥ 1.2). Error bars represent the standard error of the mean.

3.3 Vertical partitioning of aerosol properties.

In this section, we present and analyze the results of the vertical partitioning of aerosol properties, utilizing the model-derived extinction ratio as outlined in Section 2.7.1. Through this method, we made comparisons between the optical

properties of aerosols residing in the FT and those in the TC, providing insights into the distribution of aerosols across the two layers.

3.3.1 Free Tropospheric Aerosol Loading

The fraction of AOD in the free troposphere (FT AOD) relative to the total column AOD (TC AOD) over the SEA, derived from the WRF-CAM5 model, is shown in Figure 7~~8~~. For AERONET, TC AOD represents the columnar AOD above the site elevation, while for 4STAR, TC AOD refers to the AOD above the aircraft altitude. The ~~modelled~~modeled FT AOD fraction exhibits considerable spatial variation, with contributions to TC AOD ranging from 0.42 to 0.92 (mean: 0.73) at Ascension Island, 0.68 to 0.99 (mean: 0.95) for 4STAR observations, and 0.70 to 0.95 (mean: 0.86) at Namibe. Only 4STAR sky scans conducted at flight altitudes below the BL top were included in the separation, representing approximately 48% of the total 4STAR sky scans. The differences in the fraction of FT AOD between Ascension Island, 4STAR, and Namibe (as shown in Fig. 7~~8~~) can be attributed primarily to the relative proximity to the source regions. The 4STAR measurements, taken predominantly east of Ascension Island, captured denser smoke plumes before they reached the island. Additionally, the higher FT AOD in 4STAR compared to AERONET is likely due to unaccounted AOD between the aircraft altitude and the surface in the 4STAR dataset. This finding emphasizes that a substantial portion of TC AOD, exceeding 50% on average resides in the FT, indicating a higher aerosol loading in the FT compared to the MBL over the SEA. Subsequently, the model-derived fraction (Equation 4) is applied to estimate FT AOD for Ascension Island, 4STAR and Namibe retrievals using Equation (6). At Ascension Island, the mean FT AOD for the campaign period is approximately 0.23 compared to the mean TC AOD of 0.31, as shown in Figure 8~~9~~ and summarized in Table 3. However, higher mean FT AOD values of 0.35 and 0.76 are observed from 4STAR and at Namibe respectively. The FT AOD from 4STAR aligns with findings of Shinozuka et al. (2020b) who reported that daytime AOD above-cloud is similar to that in clear-sky conditions over the SEA. The observed FT aerosol loading from AERONET and 4STAR measurements over the SEA ocean agrees with the ~~modelled~~modeled FT AOD reported in Chang et al. (2023) for the same region.

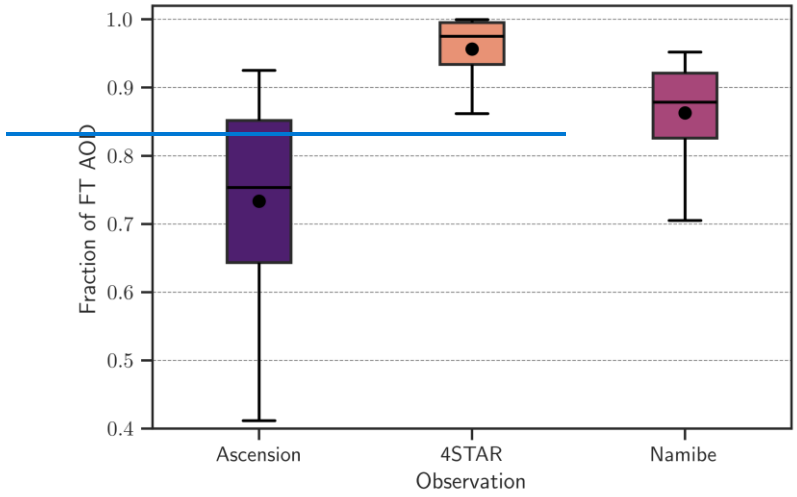

545

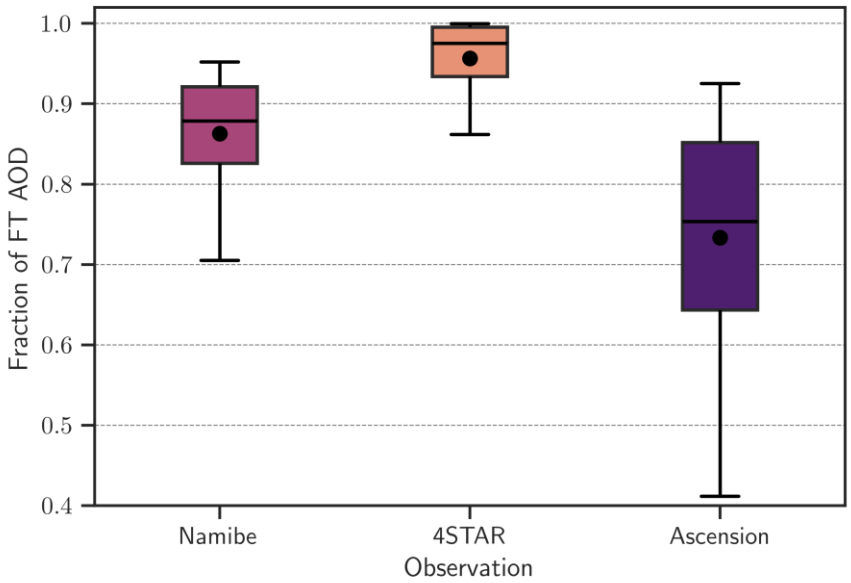

Figure 7~~8~~: Model-derived fraction of free tropospheric (FT) AOD to total column (TC) AOD. A fraction of 1 means that aerosol loading is completely in the FT. The box-whisker plot shows the 10th (lower whisker), 25th (lower box), 50th (median), 75th (upper box), and 90th (upper whisker) percentiles of fraction of FT AOD. The black circle represents the

mean fraction. Note: the outliers have been hidden in the figure. Therefore, on average, more than 50% of the aerosol loading in the ORACLES observation region is in the FT.

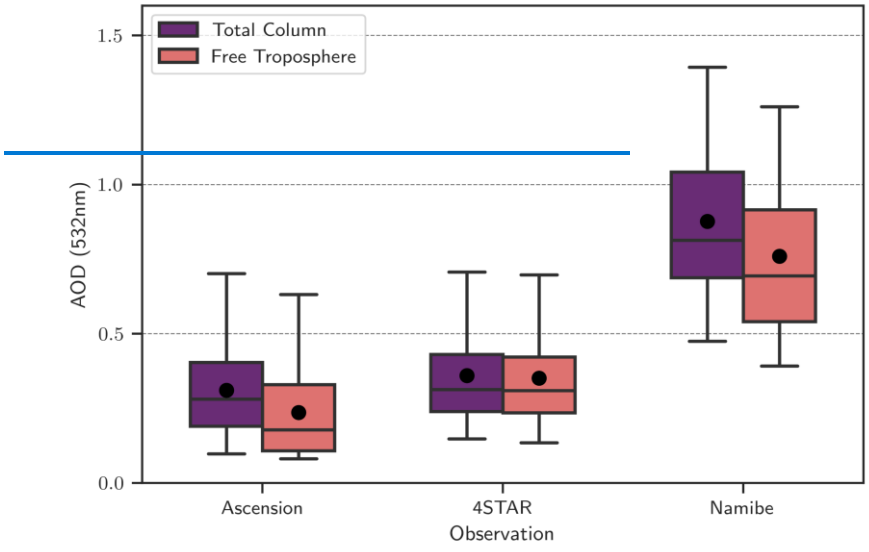
Total Column
Free Troposphere
AOD (532nm)
1.5
1.0
0.5
0.0
Ascension
4STAR
Namibe
Observation

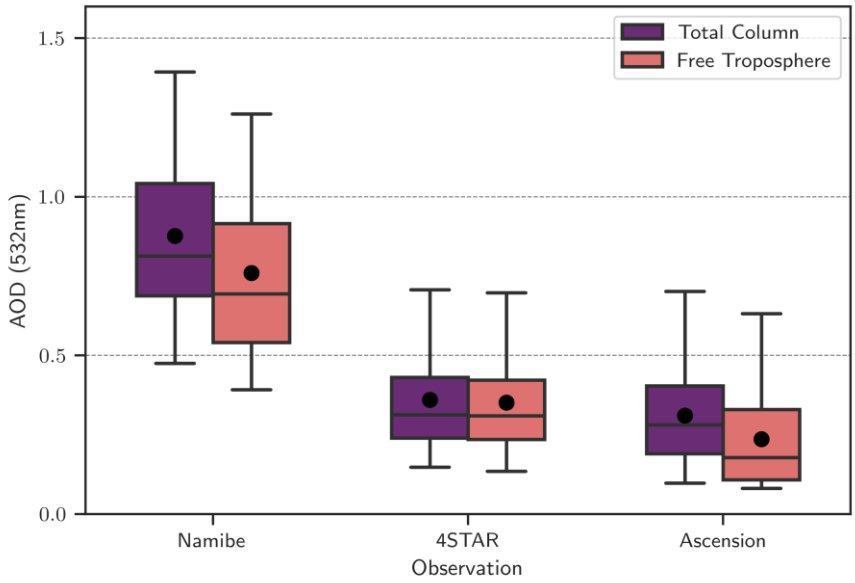
Total Column
Free Troposphere
AOD (532nm)
1.5
1.0
0.5
0.0
Namibe
4STAR
Ascension
Observation

555

Figure 89: Comparison of AOD (at 532 nm) in the total column (TC) and free troposphere (FT) over the southeast Atlantic (SEA) ocean. The box-whisker plot shows the 10th (lower whisker), 25th (lower box), 50th (median), 75th (upper box), and 90th (upper whisker) percentiles. Solid black circles represent mean AOD values.

560 **Table 3: Summary statistics of (a) Fraction of FT AOD (b) TC AOD and FT AOD (c) TC EAE and FT EAE**

(a) Fraction of FT AOD

Site Name	Count	Mean	Std	Min	25%	50%	75%	Max
Ascension	69	0.73	0.14	0.42	0.64	0.75	0.85	0.92
Namibe	133	0.86	0.07	0.70	0.82	0.88	0.92	0.95
4STAR	122	0.95	0.05	0.68	0.93	0.97	0.99	0.99

(b) TC AOD (FT AOD) 532 nm

Site Name	Count	Mean	Std	Min	25%	50%	75%	Max
Ascension	69	0.31 (0.23)	0.15 (0.15)	0.10 (0.08)	0.18 (0.10)	0.28 (0.18)	0.40 (0.33)	0.88 (0.81)
Namibe	133	0.88 (0.76)	0.28 (0.26)	0.47 (0.39)	0.69 (0.54)	0.81 (0.69)	1.04 (0.91)	1.74 (1.58)
4STAR	255	0.36 (0.35)	0.15 (0.15)	0.14 (0.13)	0.24 (0.23)	0.31 (0.30)	0.43 (0.42)	0.85 (0.84)

(c) TC EAE (FT EAE) 440-870 nm

Site Name	Count	Mean	Std	Min	25%	50%	75%	Max
Ascension	69	0.96 (0.97)	0.27 (0.28)	0.28 (0.28)	0.74 (0.75)	0.96 (0.97)	1.18 (1.20)	1.52 (1.54)
Namibe	133	1.54 (1.55)	0.15 (0.15)	1.01 (1.01)	1.47 (1.47)	1.56 (1.57)	1.64 (1.65)	1.82 (1.83)
4STAR	255	1.69 (1.70)	0.15 (0.15)	0.86 (0.86)	1.63 (1.63)	1.71 (1.71)	1.78 (1.78)	2.08 (2.08)

3.3.2 Free Tropospheric Extinction Ångstrom Exponent

The FT EAE values observed from 4STAR range between approximately 1.0 and 2.1, averaging 1.7, consistent with findings from LeBlanc et al. (2020), that reported minimal spatial dependence of above-cloud EAE in the SEA. At Namibe, FT EAE ranges from 1.0 – 1.82 with mean of about 1.55.

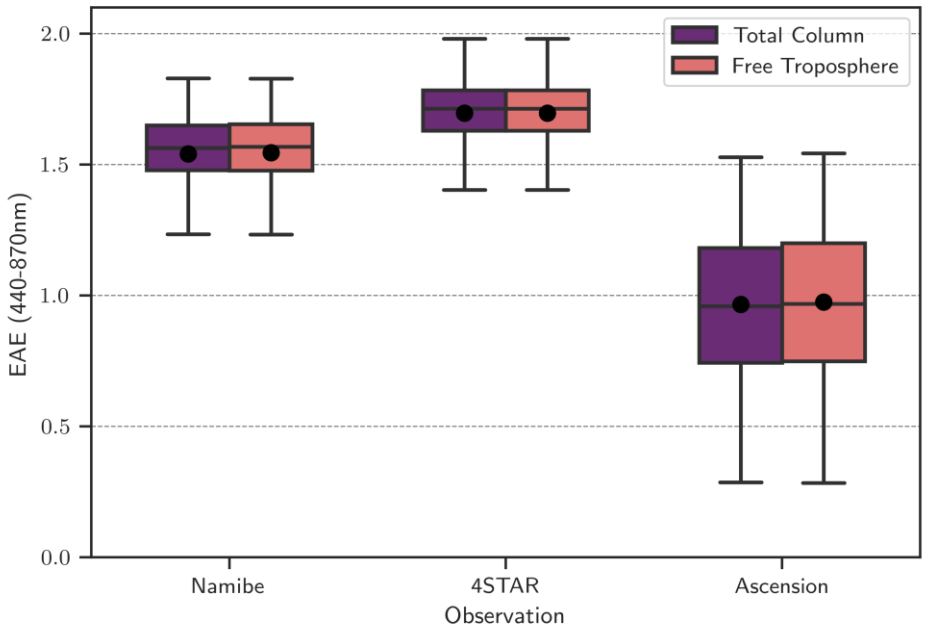

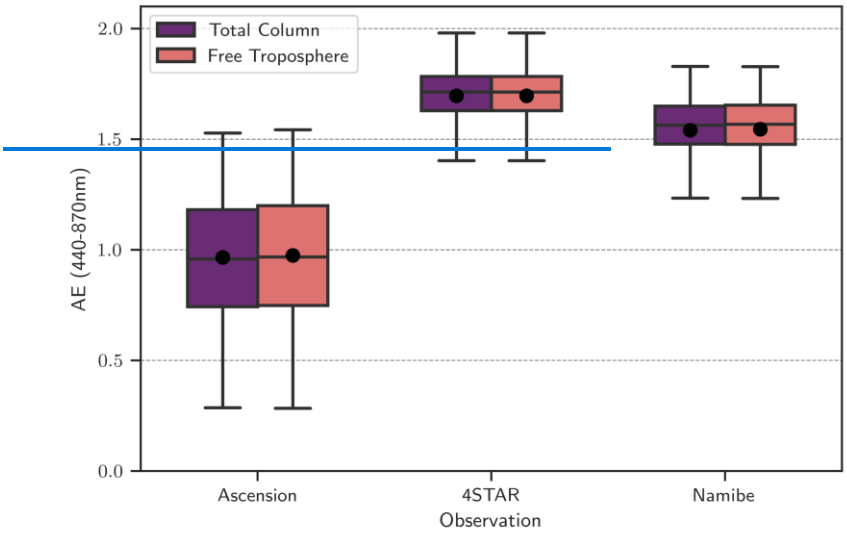

Figure 9~~10~~: Same as Figure 8 but for EAE (440-870 nm)

At Ascension Island, the FT EAE ranges from 0.28 to 1.5 with a mean of approximately 1.0, indicating a variety of particle sizes. The EAE distribution within the FT mirrors the EAE values obtained from the TC, suggesting that the particles' intensive properties remain largely unchanged after isolating MBL contributions. Typically, TC AOD at Ascension that includes the other aerosol contribution would be expected to result in a lower EAE value than the FT AOD-derived value of EAE due to the presence of sea salt aerosols and dimethyl sulfide (DMS) in the maritime environment (Smirnov et al., 2002). However, the lower FT EAE values at ~~ASI~~ Ascension Island suggest there is a source of advected coarse particles in the FT, especially for cases with FT EAE as low as 0.5 shown in Fig. 9~~10~~. The FT EAE values from 4STAR in the ORACLES campaign region primarily reflect the characteristics of BBA, with mean EAE values greater than 1.2 (Table 3), consistent with previous studies in the region (LeBlanc et al., 2020; Pistone et al., 2019).

3.3.3 Free Tropospheric Single Scattering Albedo

Figure 1~~0~~0 shows the distribution of SSA, EAE and aerosol age in the free troposphere by observation site. Over the SEA, the FT SSA differs from that of the TC SSA (shown in Figure 4~~6~~). At Namibe, the mean FT SSA is 0.85, from a range of 0.79 – 0.94. 4STAR observations show FT SSA values between 0.67 - 0.96, with a mean of 0.86. At Ascension Island, the FT SSA ranged from 0.60 - 0.98, with mean of 0.82 (Table 4). These values of FT SSA are lower than TC SSA due to exclusion of the BL portion of the TC, which may include other non-BBA aerosols with higher SSA. This difference between FT SSA and TC SSA over the SEA is further discussed in section 3.4. Given

590 that there was no vertical partitioning in the source region since BBA dominates the full column, the FT SSA and TC SSA are equal.

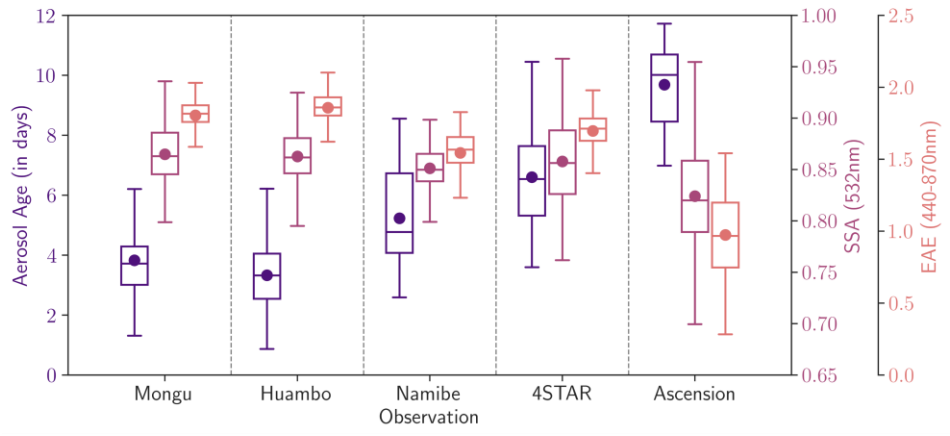

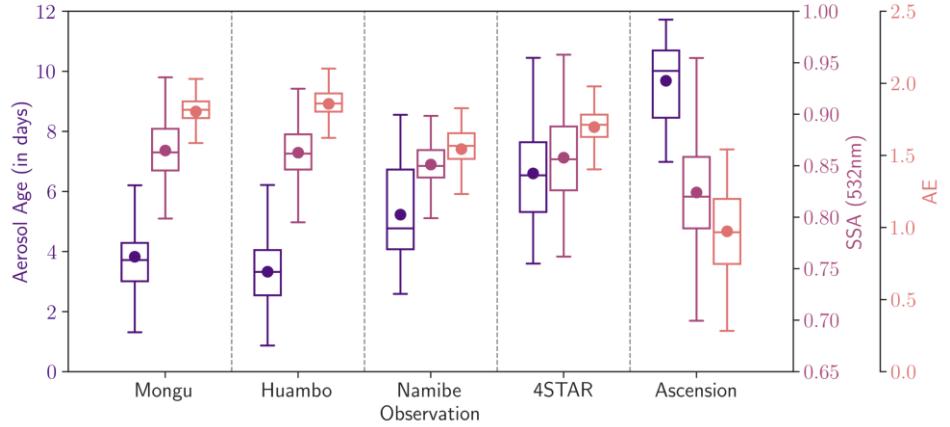

Figure 10~~4~~: Same as in Figure ~~4~~6, but for the free troposphere (FT).

595

Table 4: Summary statistics of TC and FT (in parentheses) aerosol age (a), SSA (b) and EAE (c) based on observations site

a. Result Age

Site Name	Count	Mean	Std	Min	25%	50%	75%	Max
Ascension	69	9.77 (9.68)	1.16 (1.32)	7.77 (6.98)	8.99 (8.45)	9.97 (10.02)	10.7 (10.69)	11.73 (11.73)
Namibe	133	5.82 (5.23)	1.49 (1.55)	2.82 (2.59)	5.00 (4.08)	5.59 (4.78)	7.25 (6.73)	9.05 (8.55)
Huambo	336	3.33	1.10	0.87	2.54	3.32	4.05	6.80
Mongu	355	3.83	1.25	1.09	3.01	3.72	4.29	7.55
4STAR	255	6.69 (6.60)	1.76 (1.72)	3.60 (3.60)	5.37 (5.32)	6.58 (6.54)	7.96 (7.64)	11.56 (11.78)

b. Single Scattering Albedo (SSA 532 nm)

Site Name	Count	Mean	Std	Min	25%	50%	75%	Max
Ascension	69	0.87 (0.82)	0.04 (0.07)	0.78 (0.60)	0.85 (0.79)	0.87 (0.82)	0.90 (0.86)	0.99 (0.98)
Namibe	133	0.87 (0.85)	0.02 (0.02)	0.83 (0.79)	0.86 (0.84)	0.87 (0.85)	0.88 (0.86)	0.95 (0.94)
Huambo	336	0.86	0.02	0.78	0.85	0.86	0.88	0.92
Mongu	355	0.86	0.03	0.77	0.84	0.86	0.89	0.97
4STAR	255	0.86 (0.86)	0.04 (0.05)	0.67 (0.67)	0.83 (0.82)	0.85 (0.85)	0.89 (0.88)	0.96 (0.96)

c. Extinction Angstrom Exponent (EAE 440-870 nm)

Site Name	Count	Mean	Std	Min	25%	50%	75%	Max
Ascension	69	0.96 (0.97)	0.27 (0.28)	0.28 (0.28)	0.74 (0.75)	0.96 (0.97)	1.18 (1.20)	1.52 (1.54)
Namibe	133	1.54 (1.55)	0.15 (0.15)	1.01 (1.01)	1.47 (1.47)	1.56 (1.57)	1.64 (1.65)	1.82 (1.83)
Huambo	336	1.86	0.11	0.95	1.80	1.86	1.93	2.10
Mongu	355	1.81	0.11	1.33	1.76	1.81	1.87	2.05
4STAR	255	1.69 (1.70)	0.15 (0.15)	0.86 (0.86)	1.63 (1.63)	1.71 (1.71)	1.78 (1.78)	2.08 (2.08)

3.4 Evolution of BBA SSA with age in the free troposphere

To further filter out larger particles~~, likely non-BBA~~ within the free troposphere, particularly over Ascension Island, we applied a threshold of EAE ≥ 1.2 to the FT dataset, allowing us to focus our analysis on the temporal evolution of FT SSA during BBA-laden episodes. Our findings in Fig. 1~~2~~ show a progressive increase in mean FT SSA from 0.84 to 0.87 as the aerosols age from 0 to 8 days. After 8 days, FT SSA ~~continually~~ decreases from 0.87, reaching 0.84 after approximately 12 days of transport. This ~~evolution~~ trend ~~of~~ in the mean FT SSA ~~per~~ across age bins, summarized in Table 5, begins at 0.84 (0-2 days), increases to 0.857 (2-4 days), 0.862 (4-6 days), and peaks at 0.871 (6-8 days), before declining to 0.84 (8-10 days) and 0.845 (10-12 days). However, it is important to note the higher uncertainty in FT SSA for the 10-12 day age bin due to the reduced sample size following the EAE filtering (Table 5). We analyzed the contribution of FT SSA from each campaign month to the age bins after filtering (see Table S1 and S2).

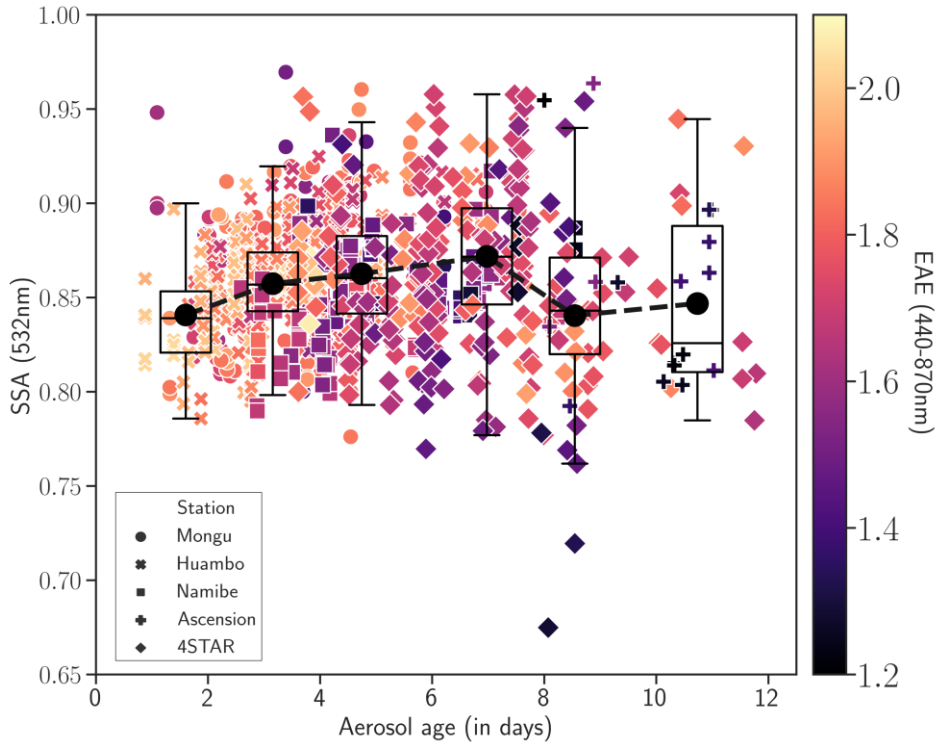

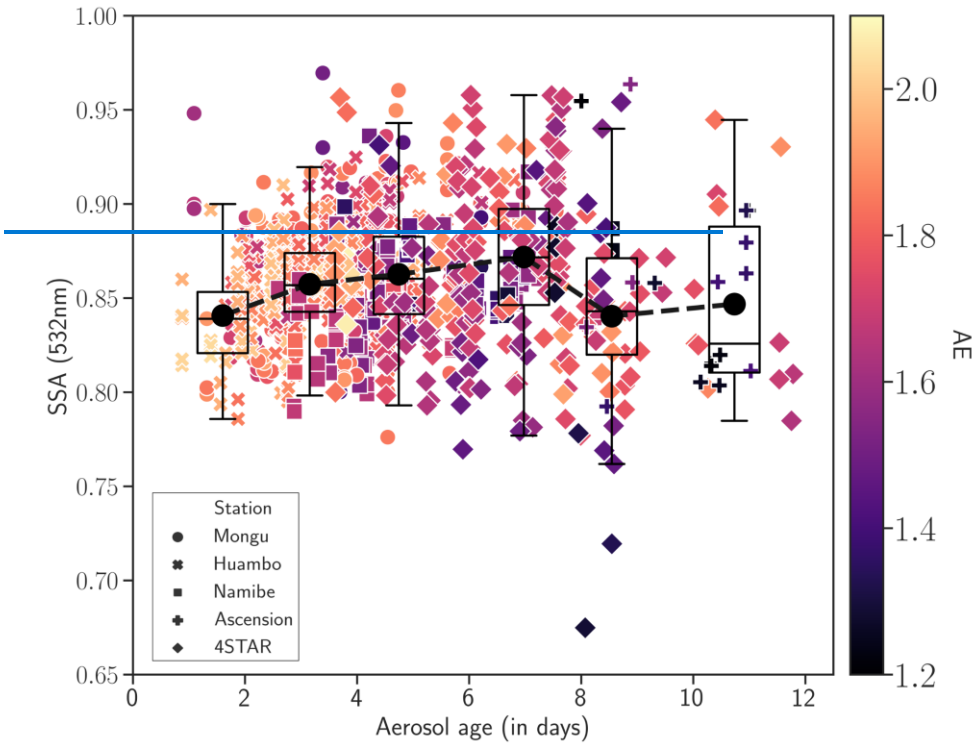

Figure 112: Evolution of FT SSA as a function of aerosol age for the optimal threshold (EAE ≥ 1.2). Scatterplot shows the relationship between SSA, EAE and aerosol age for each observation. The box-whisker plots illustrate the distribution of SSA for the categorized aerosol age bins: [0-2], [2-4], [4-6], [6-8], [8-10], [10-12], showing the 10th (lower whisker), 25th (lower box), 50th (median), 75th (upper box), and 90th (upper whisker) percentiles. The mean FT SSA for each age bin is represented in the black circles.

The analysis showed that for October (2018), there are no observations in the 10-12 day bin and only (3) data points in the 8-10 day bin. In the 8-10 day bin, retrievals are nearly evenly distributed between August (2017) and September (2016), while in the 10-12 day bin, the ratio of September to August retrievals is approximately 3:1. The total number (3) of observations from October (2018) in the 8-10 day bin (3) and 10-12 day bin (0) represent less than 2% of total observations (229) for that year. Meanwhile, the contribution (27) from August (2017) and (42) from September (2016) represent about 5% and 16% of the total observations (556 and 258, respectively) for the years. This distribution of observations in the 8-10 and 10-12 day bins suggests that the decrease in SSA observed for older aerosol plumes is not due to an overrepresentation of August data, which climatological studies suggest exhibit lower SSA due to their emissions earlier in the burning season. However, other factors, rather than the timing of the emission, drive the observed SSA change in aged plumes. ~~the following: no October (2018) retrievals are present in the 10-12 day age bin, and only a few are found in the 8-10 day bin; the 8-10 day bin contains a relatively equal distribution of retrievals~~

~~between August and September; and in the 10-12 day bin, the ratio of September to August retrievals is approximately 3:1. These distributions show that the observed decrease in SSA within the 8-10 and 10-12 day age bins, compared to younger plume ages, is not driven by overrepresentation of August data, earlier in the burning season, for which prior studies have identified climatologically lower SSA in the region. This is significant, as it implies that other factors, rather than the timing of the emission, drive the observed SSA change in aged plumes.~~

The maximum value of mean FT SSA at 6-8 days shows that the BBA absorptivity decreases as the aerosol ages from emission to about 6-8 days. After 6-8 days, the FT SSA decreases, indicating that older BBA are more efficient at absorbing solar radiation. This evolution of FT SSA supports the observations from previous studies where it was reported that the SSA initially increases within a few hours of emission and peaks on the fourth day before decreasing (Sedlacek et al., 2022). The results presented here also support the findings from Dobracki et al. (2023) who showed that in the ORACLES region, SSA decreases as ~~the~~ aerosol~~s~~ age~~s~~ because of a reduction in organic aerosol mass concentrations.

Table 5: Summary statistics of TC SSA and FT SSA (in parentheses) for each age group at (EAE ≥ 1.2)

Age Group	Count	Mean	Std	Min	25%	50%	75%	Max	SE
0-2	47	0.841	0.03	0.785	0.820	0.840	0.853	0.948	0.004
	(47)	(0.84)	(0.03)	(0.785)	(0.820)	(0.840)	(0.853)	(0.948)	(0.004)
2-4	425	0.859	0.02	0.795	0.845	0.859	0.874	0.960	0.001
	(430)	(0.857)	(0.03)	(0.790)	(0.843)	(0.857)	(0.874)	(0.96)	(0.001)
4-6	319	0.868	0.03	0.776	0.847	0.865	0.887	0.960	0.001
	(327)	(0.862)	(0.03)	(0.769)	(0.841)	(0.860)	(0.882)	(0.960)	(0.001)
6-8	169	0.871	0.04	0.778	0.847	0.873	0.895	0.958	0.003
	(167)	(0.871)	(0.04)	(0.777)	(0.846)	(0.871)	(0.897)	(0.958)	(0.003)
8-10	64	0.861	0.05	0.675	0.829	0.860	0.896	0.970	0.007
	(49)	(0.840)	(0.05)	(0.675)	(0.820)	(0.843)	(0.871)	(0.963)	(0.008)
10-12	16	0.858	0.04	0.802	0.827	0.843	0.901	0.944	0.011
	(23)	(0.845)	(0.04)	(0.785)	(0.810)	(0.825)	(0.890)	(0.944)	(0.009)

We examined the mean FT SSA against the mean TC SSA at the established optimal EAE threshold (Fig. 1~~2~~3) to gain a clearer understanding of the evolution of SSA shown in Fig. 1~~1~~2 and to highlight the significance of employing the combination of the model-based vertical extinction separation with an EAE filter. The results demonstrate that FT SSA decreases by more than 2% for BBA aged beyond 8 days. This decrease in mean FT SSA compared to TC SSA suggests that by combining the two methods described in section 2.7, we are able to achieve our desired isolation of fine, BBA particles in the FT from the contribution of larger (EAE < 1.2), non-absorbing aerosols. Applying the EAE filtering solely to the TC data removed larger particles but did not account for other less absorbing fine particles, from mixing of BBA with marine aerosols with the boundary layer (Dang et al., 2022), or non-absorbing

fine-mode marine aerosols (Fitzgerald, 1991). However, the application of the EAE filtering to the FT data after partitioning efficiently isolate all non-BBA particles. ~~This decrease in mean FT SSA compared to TC SSA is consistent with the desired isolation of fine, absorbing BBA in the FT and suggests that applying only an AE filter to the TC observations isolates the contribution of larger particles. However, the AE filter does not fully isolate less-absorbing fine particles, which could include BBA mixed with scattering marine aerosols within the boundary layer, as shown by Dang et al. (2022), or non-absorbing fine-mode marine aerosols (Fitzgerald, 1991).~~ Overall, the combined use of both techniques, reveals a distinct evolution pattern of BBA in the FT. To examine the sensitivity of our assumption that SSA_{BL} = 1, we tested alternative SSA_{BL} values to account for varying degrees of absorption within the BL. The results showed an evolution of FT SSA similar to that in Figure 12~~3~~, with a decrease in ~~mean~~ the mean FT SSA after 8 days (supplemental Figure S6).

The changes in SSA presented in this study are primarily associated with chemical and physical processes in the atmosphere (Dobracki et al., 2023). Fresh aerosols over the continent show a low SSA, likely a result of a high proportion of rBC from flaming fires. As these aerosols age in the atmosphere, they accumulate organic coatings, a process that concurrently occurs with homogeneous nucleation of secondary organic aerosol (SOA) from volatile organic compounds (VOCs). These processes happen rapidly within hours and continue for the first few days (Hodshire et al., 2019; Sedlacek et al., 2022), increasing the contribution of OA to the aging particles, thereby increasing SSA. After 6-8 days, the SSA starts to decrease, possibly due to lensing enhancement or a reduction in the production of SOA. Additionally, heterogeneous oxidation may drive the repartition of aerosol mass back into gas phase. In addition to compositional changes in BBA driven by accumulation and/or evaporation of organic coatings, a concurrent change in fine-mode particle size is also likely during aging. These size changes are possibly a consequence of the same chemical processes and contribute to the observed trends in optical properties. For instance, as particles shrink, their scattering efficiency decreases, which in turn can lead to a reduction in SSA. ~~because SOA production slows down and heterogeneous oxidation repartitions some of the aerosol mass back into the gas phase. In addition to changes in BBA composition from accumulation and/or evaporation of organic coatings, there is likely some concurrent change in fine mode particle size that occurs in these aging processes. Fine mode scattering efficiency deceases as fine mode particle size decreases and this also can result in lower SSA for the smaller particles.~~

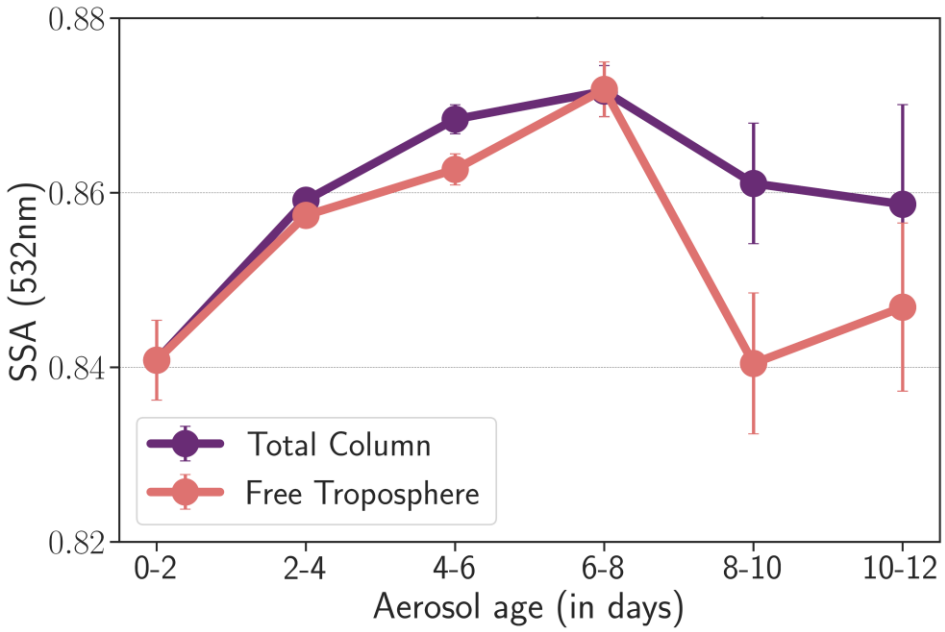

Figure 1~~3~~2: Comparison between evolution of TC SSA and evolution of FT SSA for all the aerosol age bin at the optimal threshold (EAE ≥ 1.2). Error bars represent the standard error of the mean.

4 Conclusions

We introduce a novel approach to investigate the evolution of optical properties of BBA during long-range transport from continental southern Africa to the SEA region. This approach integrates ground-based and airborne remote sensing measurements from AERONET and 4STAR, collected during the three ORACLES deployments, with model output from two WRF configurations: WRF-CAM5 and WRF-AAM, to extend the scope for studying aerosol evolution. Our analysis primarily focuses on examining the variations in observed SSA and AE in relation to the ~~modelled~~modeled age of the aerosols. This work is unique and builds upon the previous research over the SEA by including AERONET observations over land which allows for a more spatially extensive study of BBA evolution than those prior.

The WRF-AAM model, utilizing CO tracers, provided estimates of the aerosol age (defined as time elapsed since emission). We were able to assess how BBA optical properties evolved during long-range transport over the SEA by tracking the CO tracers in the model for a period of 2 weeks. Our result showed a longitudinal variation in SSA, that corresponds with the model-derived aerosol age and aligns with the transport pathway from the continent. The results revealed that SSA generally increased as BBA were transported away from the emission source, with lower SSA values measured at the Mongu and Huambo sites than those measured at the coastal Namibe site.

Throughout 2016, 2017, and 2018, there was a clear trend in mean SSA values, generally increasing with distance from the emission source while over land, with low values recorded at Mongu and Huambo, and the highest observed near the central African coast.

We next applied a model-based vertical separation and AE-based threshold to focus our analysis on the upper-level BBA observations over the SEA. Our analysis showed a distinct temporal trend in FT SSA, where mean FT SSA values initially increased from 0.84 to 0.87 during the first 7 days following emission, followed by a decline back to 0.84 after about 12 days. This implies that the observed aerosol aging led to a 0.03 change in SSA, a trend consistent with in-situ measurements reported during the ORACLES campaign by Sedlacek et al. (2022) and Dobracki et al. (2023). In Dobracki et al. (2023), a similar SSA change of approximately 0.06 was observed following a concomitant reduction in OA:BC mass ratio. Given that a variation of ±0.03 in SSA can result in a difference of up to ~20 Wm^{-2} in local direct radiative effect (Wilcox, 2012), the observed SSA changes in our analysis can have substantial effects on Earth's radiative budget, particularly in the SEA, especially considering the influence of BBA above clouds on the sign and magnitude of TOA forcing over dark ocean surface, as noted by Keil and Haywood (2003). To our knowledge, this study is the first to use remote sensing observations to document changes in BBA properties during long-range transport and associated aging.

We conclude from our analysis that BBA undergo variations in their optical properties that have important implications for the radiation balance. Upon emission, BBA are characterized by low SSA values (high absorptivity), and elevated AE values, indicating the prevalence of small sized particles. During initial stages of transport, BBA SSA increases, signifying a reduction absorptivity, accompanied by a decrease in AE, indicative of particle growth. However, there is a subsequent decrease in SSA (increase in absorptivity) as BBA continue to age during extended transport. This evolution is driven by atmospheric processes. Dobracki et al. (2023) attributed these changes in SSA to various chemical and physical transformation of BBA in the atmosphere.

These results, in agreement with the findings of Dobracki et al. (2023) and Sedlacek et al. (2022), emphasize the continuous evolution of BBA optical properties, influenced by changes in their chemical and microphysical properties. Accurately capturing these evolving properties throughout their lifecycle represents the next step for improving model fidelity and predictive capability. To the best of our knowledge, this study is among the first efforts to investigate BBA evolution over an extended temporal scale, spanning weeks, using columnar observations from remote sensing.

The data analysis techniques and findings from this study contribute to a greater understanding of how BBA optical properties change and the radiative effects associated with those changes. This research also provides further insight into the spatial and temporal evolution of BBA. More importantly, the changes in BBA optical properties associated with aging documented here and elsewhere will need to be incorporated into ESMs to properly represent BBA aerosol properties and effects, and to properly predict future changes in BBA climatic impacts.

Data Availability:

The NASA P-3 aircraft data was published by ORACLES Science Team (2021) and can be accessed at these links:
ORACLES 2016: https://doi.org/10.5067/Suborbital/ORACLES/P3/2016_V3;
ORACLES 2017: https://doi.org/10.5067/Suborbital/ORACLES/P3/2017_V3;
ORACLES 2018: https://doi.org/10.5067/Suborbital/ORACLES/P3/2018_V3;
AERONET inversion products are available at https://aeronet.gsfc.nasa.gov/

Author Contributions

This study was conceptualized by JR. JR, CJF and AAF formulated the methodology. PES and CH ran the WRF simulations and provided model output. KP, SEL, MSR operated the 4STAR instrument aboard the P-3 aircraft and processed the 4STAR data. LM contributed to the processing of 4STAR retrievals. AAF organized all datasets, performed analyses, and visualized the results. PG and EL are the PIs for the AERONET network. JR and PZ led efforts to acquire funding and were the PIs for the ORACLES mission. AAF wrote the draft with contributions from all authors.

Competing Interests

At least one of the (co-)authors is a member of the editorial board of Atmospheric Chemistry and Physics.

Acknowledgements

Portions of the computational work for this paper were supported by and conducted using resources at the University of Oklahoma (OU) Supercomputing Center for Education & Research (OSCER). We extend our gratitude to the entire NASA ORACLES team for their successful deployment. Our thanks also go to the site PIs and managers for the AERONET stations at Mongu, Huambo, Namibe and Ascension Island. Data analysis and visualization were carried out using open-source libraries in MATLAB and Python.

Financial Support

This research has been supported by the University of Oklahoma (OU) start-up package (grant no. 122007900). The ORACLES field campaign was funded through the NASA Earth Venture Suborbital-2 program (grant no. NNH13ZDA001N-EVS2). PZ acknowledges funding support from DOE ASR award DE-SC0021250.

References

Abel, S. J., Haywood, J. M., Highwood, E. J., Li, J., & Buseck, P. R. (2003). Evolution of biomass burning aerosol properties from an agricultural fire in southern Africa. *Geophysical Research Letters*, *30*(15). https://doi.org/https://doi.org/10.1029/2003GL017342

Ackerman, A. S., Toon, O. B., Taylor, J. P., Johnson, D. W., Hobbs, P. V., & Ferek, R. J. (2000). Effects of Aerosols on Cloud Albedo: Evaluation of Twomey's Parameterization of Cloud Susceptibility Using Measurements of Ship Tracks. *Journal of the Atmospheric Sciences*, *57*(16), 2684-2695. https://doi.org/10.1175/1520-0469(2000)057<2684:Eoaoca>2.0.Co;2

Adachi, K., & Buseck, P. R. (2015). Changes in shape and composition of sea-salt particles upon aging in an urban atmosphere. *Atmospheric Environment*, *100*, 1-9. https://doi.org/https://doi.org/10.1016/j.atmosenv.2014.10.036

Adebiyi, A. A., & Zuidema, P. (2016). The role of the southern African easterly jet in modifying the southeast Atlantic aerosol and cloud environments. *Quarterly Journal of the Royal Meteorological Society*, *142*(697), 1574-1589. https://doi.org/https://doi.org/10.1002/qj.2765

Adebiyi, A. A., Zuidema, P., & Abel, S. J. (2015). The Convolution of Dynamics and Moisture with the Presence of Shortwave Absorbing Aerosols over the Southeast Atlantic. *Journal of Climate*, *28*(5), 1997-2024. https://doi.org/10.1175/jcli-d-14-00352.1

Aladodo, S. S., Akoshile, C. O., Ajibola, T. B., Sani, M., Iborida, O. A., & Fakoya, A. A. (2022). Seasonal Tropospheric Aerosol Classification Using AERONET Spectral Absorption Properties in African Locations. *Aerosol Science and Engineering*, *6*(3), 246-266. https://doi.org/10.1007/s41810-022-00140-x

Albrecht, B. A. (1989). Aerosols, Cloud Microphysics, and Fractional Cloudiness. *Science*, *245*(4923), 1227-1230. https://doi.org/doi:10.1126/science.245.4923.1227

Alexander, D. T. L., Crozier, P. A., & Anderson, J. R. (2008). Brown Carbon Spheres in East Asian Outflow and Their Optical Properties. *Science*, *321*(5890), 833-836. https://doi.org/doi:10.1126/science.1155296

Andreae, M. O., & Gelencsér, A. (2006). Black carbon or brown carbon? The nature of light-absorbing carbonaceous aerosols. *Atmos. Chem. Phys.*, *6*(10), 3131-3148. https://doi.org/10.5194/acp-6-3131-2006

Andreae, M. O., & Rosenfeld, D. (2008). Aerosol–cloud–precipitation interactions. Part 1. The nature and sources of cloud-active aerosols. *Earth-Science Reviews*, *89*(1), 13-41. https://doi.org/https://doi.org/10.1016/j.earscirev.2008.03.001

Baars, H., Radenz, M., Floutsi, A. A., Engelmann, R., Althausen, D., Heese, B., Ansmann, A., Flament, T., Dabas, A., Trapon, D., Reitebuch, O., Bley, S., & Wandinger, U. (2021). Californian Wildfire Smoke Over Europe: A First Example of the Aerosol Observing Capabilities of Aeolus Compared to Ground-Based Lidar. *Geophysical Research Letters*, *48*(8), e2020GL092194. https://doi.org/https://doi.org/10.1029/2020GL092194

Bellouin, N., Quaas, J., Gryspeerdt, E., Kinne, S., Stier, P., Watson-Parris, D., Boucher, O., Carslaw, K. S., Christensen, M., Daniau, A.-L., Dufresne, J.-L., Feingold, G., Fiedler, S., Forster, P., Gettelman, A., Haywood, J. M., Lohmann, U., Malavelle, F., Mauritsen, T.,…Stevens, B. (2020). Bounding Global Aerosol Radiative Forcing of Climate Change. *Reviews of Geophysics*, *58*(1), e2019RG000660. https://doi.org/https://doi.org/10.1029/2019RG000660

Bergstrom, R. W., Pilewskie, P., Russell, P. B., Redemann, J., Bond, T. C., Quinn, P. K., & Sierau, B. (2007). Spectral absorption properties of atmospheric aerosols. *Atmos. Chem. Phys.*, *7*(23), 5937-5943. https://doi.org/10.5194/acp-7-5937-2007

Bond, T. C., Doherty, S. J., Fahey, D. W., Forster, P. M., Berntsen, T., DeAngelo, B. J., Flanner, M. G., Ghan, S., Kärcher, B., Koch, D., Kinne, S., Kondo, Y., Quinn, P. K., Sarofim, M. C., Schultz, M. G.,

Schulz, M., Venkataraman, C., Zhang, H., Zhang, S.,…Zender, C. S. (2013). Bounding the role of black carbon in the climate system: A scientific assessment. *Journal of Geophysical Research: Atmospheres*, *118*(11), 5380-5552. https://doi.org/10.1002/jgrd.50171

Bond, T. C., Habib, G., & Bergstrom, R. W. (2006). Limitations in the enhancement of visible light absorption due to mixing state. *Journal of Geophysical Research: Atmospheres*, *111*(D20).

Bond, T. C., Streets, D. G., Yarber, K. F., Nelson, S. M., Woo, J.-H., & Klimont, Z. (2004). A technology-based global inventory of black and organic carbon emissions from combustion. *Journal of Geophysical Research: Atmospheres*, *109*(D14). https://doi.org/https://doi.org/10.1029/2003JD003697

Boucher, O. (2015). Atmospheric Aerosols. In *Atmospheric Aerosols: Properties and Climate Impacts* (pp. 9-24). Springer Netherlands. https://doi.org/10.1007/978-94-017-9649-1_2

Boucher, O., Randall, D., Artaxo, P., Bretherton, C., Feingold, G., Forster, P., Kerminen, V.-M., Kondo, Y., Liao, H., Lohmann, U., Rasch, P., Satheesh, S., Sherwood, S., Stevens, B., & Zhang, X. (2013). Clouds and Aerosols. In I. P. o. C. Change (Ed.), *Climate Change 2013: The Physical Science Basis. Contribution of Working Group I to the Fifth Assessment Report of the Intergovernmental Panel on Climate Change* (pp. 571-892). Cambridge University Press. https://doi.org/10.1017/CBO9781107415324.016.

Bowman, D. M. J. S., Balch, J. K., Artaxo, P., Bond, W. J., Carlson, J. M., Cochrane, M. A., D'Antonio, C. M., DeFries, R. S., Doyle, J. C., Harrison, S. P., Johnston, F. H., Keeley, J. E., Krawchuk, M. A., Kull, C. A., Marston, J. B., Moritz, M. A., Prentice, I. C., Roos, C. I., Scott, A. C.,…Pyne, S. J. (2009). Fire in the Earth System. *Science*, *324*(5926), 481-484. https://doi.org/doi:10.1126/science.1163886

Bretherton, C. S., & Park, S. (2009). A New Moist Turbulence Parameterization in the Community Atmosphere Model. *Journal of Climate*, *22*(12), 3422-3448. https://doi.org/10.1175/2008jcli2556.1

Brown, H., Liu, X., Pokhrel, R., Murphy, S., Lu, Z., Saleh, R., Mielonen, T., Kokkola, H., Bergman, T., Myhre, G., Skeie, R. B., Watson-Paris, D., Stier, P., Johnson, B., Bellouin, N., Schulz, M., Vakkari, V., Beukes, J. P., van Zyl, P. G.,…Chand, D. (2021). Biomass burning aerosols in most climate models are too absorbing. *Nat Commun*, *12*(1), 277. https://doi.org/10.1038/s41467-020-20482-9

Campbell, P., Zhang, Y., Wang, K., Leung, R., Fan, J., Zheng, B., Zhang, Q., & He, K. (2017). Evaluation of a multi-scale WRF-CAM5 simulation during the 2010 East Asian Summer Monsoon. *Atmospheric Environment*, *169*, 204-217. https://doi.org/https://doi.org/10.1016/j.atmosenv.2017.09.008

Chand, D., Wood, R., Anderson, T. L., Satheesh, S. K., & Charlson, R. J. (2009). Satellite-derived direct radiative effect of aerosols dependent on cloud cover. *Nature Geoscience*, *2*(3), 181-184. https://doi.org/10.1038/ngeo437

Chang, I., & Christopher, S. A. (2017). The impact of seasonalities on direct radiative effects and radiative heating rates of absorbing aerosols above clouds. *Quarterly Journal of the Royal Meteorological Society*, *143*(704), 1395-1405. https://doi.org/https://doi.org/10.1002/qj.3012

Chang, I., Gao, L., Flynn, C. J., Shinozuka, Y., Doherty, S. J., Diamond, M. S., Longo, K. M., Ferrada, G. A., Carmichael, G. R., Castellanos, P., da Silva, A. M., Saide, P. E., Howes, C., Xue, Z., Mallet, M., Govindaraju, R., Wang, Q., Cheng, Y., Feng, Y.,…Redemann, J. (2023). On the differences in the vertical distribution of modeled aerosol optical depth over the southeastern Atlantic. *Atmos. Chem. Phys.*, *23*(7), 4283-4309. https://doi.org/10.5194/acp-23-4283-2023

Che, H., Stier, P., Gordon, H., Watson-Parris, D., & Deaconu, L. (2021). Cloud adjustments dominate the overall negative aerosol radiative effects of biomass burning aerosols in UKESM1 climate model simulations over the south-eastern Atlantic. *Atmos. Chem. Phys.*, *21*(1), 17-33. https://doi.org/10.5194/acp-21-17-2021

Chylek, P., & Wong, J. (1995). Effect of absorbing aerosols on global radiation budget. *Geophysical Research Letters*, *22*(8), 929-931. https://doi.org/https://doi.org/10.1029/95GL00800

Collier, S., Zhou, S., Onasch, T. B., Jaffe, D. A., Kleinman, L., Sedlacek, A. J., III, Briggs, N. L., Hee, J., Fortner, E., Shilling, J. E., Worsnop, D., Yokelson, R. J., Parworth, C., Ge, X., Xu, J., Butterfield, Z., Chand, D., Dubey, M. K., Pekour, M. S.,…Zhang, Q. (2016). Regional Influence of Aerosol Emissions from Wildfires Driven by Combustion Efficiency: Insights from the BBOP Campaign. *Environmental Science & Technology*, *50*(16), 8613-8622. https://doi.org/10.1021/acs.est.6b01617

Dang, C., Segal-Rozenhaimer, M., Che, H., Zhang, L., Formenti, P., Taylor, J., Dobracki, A., Purdue, S., Wong, P. S., Nenes, A., Sedlacek Iii, A., Coe, H., Redemann, J., Zuidema, P., Howell, S., & Haywood, J. (2022). Biomass burning and marine aerosol processing over the southeast Atlantic Ocean: a TEM single-particle analysis. *Atmos. Chem. Phys.*, *22*(14), 9389-9412. https://doi.org/10.5194/acp-22-9389-2022

Darmenov, A. S., & da Silva, A. (2015). *The Quick Fire Emissions Dataset (QFED): Documentation of versions 2.1, 2.2 and 2.4* (Technical Report Series on Global Modeling and Data Assimilation, Issue. NASA.

de Graaf, M., Bellouin, N., Tilstra, L. G., Haywood, J., & Stammes, P. (2014). Aerosol direct radiative effect of smoke over clouds over the southeast Atlantic Ocean from 2006 to 2009. *Geophysical Research Letters*, *41*(21), 7723-7730. https://doi.org/https://doi.org/10.1002/2014GL061103

Deardorff, J. W. (1972). Parameterization of the Planetary Boundary layer for Use in General Circulation Models. *Monthly Weather Review*, *100*(2), 93-106. https://doi.org/https://doi.org/10.1175/1520-0493(1972)100<0093:POTPBL>2.3.CO;2

Dedrick, J. L., Russell, L. M., Sedlacek Iii, A. J., Kuang, C., Zawadowicz, M. A., & Lubin, D. (2024). Aerosol-Correlated Cloud Activation for Clean Conditions in the Tropical Atlantic Boundary Layer During LASIC. *Geophysical Research Letters*, *51*(3), e2023GL105798. https://doi.org/https://doi.org/10.1029/2023GL105798

Denjean, C., Bourrianne, T., Burnet, F., Mallet, M., Maury, N., Colomb, A., Dominutti, P., Brito, J., Dupuy, R., Sellegri, K., Schwarzenboeck, A., Flamant, C., & Knippertz, P. (2020a). Overview of aerosol optical properties over southern West Africa from DACCIWA aircraft measurements. *Atmos. Chem. Phys.*, *20*(8), 4735-4756. https://doi.org/10.5194/acp-20-4735-2020

Denjean, C., Brito, J., Libois, Q., Mallet, M., Bourrianne, T., Burnet, F., Dupuy, R., Flamant, C., & Knippertz, P. (2020b). Unexpected Biomass Burning Aerosol Absorption Enhancement Explained by Black Carbon Mixing State. *Geophysical Research Letters*, *47*(19), e2020GL089055. https://doi.org/https://doi.org/10.1029/2020GL089055

Diamond, M. S., Dobracki, A., Freitag, S., Small Griswold, J. D., Heikkila, A., Howell, S. G., Kacarab, M. E., Podolske, J. R., Saide, P. E., & Wood, R. (2018). Time-dependent entrainment of smoke presents an observational challenge for assessing aerosol–cloud interactions over the southeast Atlantic Ocean. *Atmos. Chem. Phys.*, *18*(19), 14623-14636. https://doi.org/10.5194/acp-18-14623-2018

Dobracki, A., Lewis, E., Sedlacek Iii, A., Tatro, T., Zawadowicz, M., & Zuidema, P. (2024). Burning conditions and transportation pathways determine biomass-burning aerosol properties in the Ascension Island marine boundary layer. *EGUsphere*, *2024*, 1-51. https://doi.org/10.5194/egusphere-2024-1347

Dobracki, A., Lewis, E. R., Sedlacek Iii, A. J., Tatro, T., Zawadowicz, M. A., & Zuidema, P. (2025). Burning conditions and transportation pathways determine biomass-burning aerosol properties in the Ascension Island marine boundary layer. *Atmos. Chem. Phys.*, *25*(4), 2333-2363. https://doi.org/10.5194/acp-25-2333-2025

Dobracki, A., Zuidema, P., Howell, S. G., Saide, P., Freitag, S., Aiken, A. C., Burton, S. P., Sedlacek Iii, A. J., Redemann, J., & Wood, R. (2023). An attribution of the low single-scattering albedo of biomass

burning aerosol over the southeastern Atlantic. *Atmos. Chem. Phys.*, *23*(8), 4775-4799. https://doi.org/10.5194/acp-23-4775-2023

Doherty, S. J., Saide, P. E., Zuidema, P., Shinozuka, Y., Ferrada, G. A., Gordon, H., Mallet, M., Meyer, K., Painemal, D., Howell, S. G., Freitag, S., Dobracki, A., Podolske, J. R., Burton, S. P., Ferrare, R. A., Howes, C., Nabat, P., Carmichael, G. R., da Silva, A.,…Redemann, J. (2022). Modeled and observed properties related to the direct aerosol radiative effect of biomass burning aerosol over the southeastern Atlantic. *Atmos. Chem. Phys.*, *22*(1), 1-46. https://doi.org/10.5194/acp-22-1-2022

Dubovik, O., Holben, B., Eck, T. F., Smirnov, A., Kaufman, Y. J., King, M. D., Tanré, D., & Slutsker, I. (2002). Variability of Absorption and Optical Properties of Key Aerosol Types Observed in Worldwide Locations. *Journal of the Atmospheric Sciences*, *59*(3), 590-608. https://doi.org/10.1175/1520-0469(2002)059<0590:Voaaop>2.0.Co;2

Dunagan, S. E., Johnson, R., Zavaleta, J., Russell, P. B., Schmid, B., Flynn, C., Redemann, J., Shinozuka, Y., Livingston, J., & Segal-Rosenhaimer, M. (2013). Spectrometer for Sky-Scanning Sun-Tracking Atmospheric Research (4STAR): Instrument Technology. *Remote Sensing*, *5*(8), 3872-3895. https://www.mdpi.com/2072-4292/5/8/3872

Eck, T. F., Holben, B. N., Reid, J. S., Dubovik, O., Smirnov, A., O'Neill, N. T., Slutsker, I., & Kinne, S. (1999). Wavelength dependence of the optical depth of biomass burning, urban, and desert dust aerosols. *Journal of Geophysical Research: Atmospheres*, *104*(D24), 31333-31349. https://doi.org/https://doi.org/10.1029/1999JD900923

Eck, T. F., Holben, B. N., Reid, J. S., Mukelabai, M. M., Piketh, S. J., Torres, O., Jethva, H. T., Hyer, E. J., Ward, D. E., Dubovik, O., Sinyuk, A., Schafer, J. S., Giles, D. M., Sorokin, M., Smirnov, A., & Slutsker, I. (2013). A seasonal trend of single scattering albedo in southern African biomass-burning particles: Implications for satellite products and estimates of emissions for the world's largest biomass-burning source. *Journal of Geophysical Research: Atmospheres*, *118*(12), 6414-6432. https://doi.org/10.1002/jgrd.50500

Eck, T. F., Holben, B. N., Ward, D. E., Mukelabai, M. M., Dubovik, O., Smirnov, A., Schafer, J. S., Hsu, N. C., Piketh, S. J., Queface, A., Roux, J. L., Swap, R. J., & Slutsker, I. (2003). Variability of biomass burning aerosol optical characteristics in southern Africa during the SAFARI 2000 dry season campaign and a comparison of single scattering albedo estimates from radiometric measurements. *Journal of Geophysical Research: Atmospheres*, *108*(D13). https://doi.org/https://doi.org/10.1029/2002JD002321

Fast, J. D., Gustafson Jr., W. I., Easter, R. C., Zaveri, R. A., Barnard, J. C., Chapman, E. G., Grell, G. A., & Peckham, S. E. (2006). Evolution of ozone, particulates, and aerosol direct radiative forcing in the vicinity of Houston using a fully coupled meteorology-chemistry-aerosol model. *Journal of Geophysical Research: Atmospheres*, *111*(D21). https://doi.org/https://doi.org/10.1029/2005JD006721

Feng, X., Wang, J., Teng, S., Xu, X., Zhu, B., Wang, J., Zhu, X., Yurkin, M. A., & Liu, C. (2021). Can light absorption of black carbon still be enhanced by mixing with absorbing materials? *Atmospheric Environment*, *253*, 118358. https://doi.org/https://doi.org/10.1016/j.atmosenv.2021.118358

Feng, Y., Ramanathan, V., & Kotamarthi, V. R. (2013). Brown carbon: a significant atmospheric absorber of solar radiation? *Atmos. Chem. Phys.*, *13*(17), 8607-8621. https://doi.org/10.5194/acp-13-8607-2013

Fitzgerald, J. W. (1991). Marine aerosols: A review. *Atmospheric Environment. Part A. General Topics*, *25*(3), 533-545. https://doi.org/https://doi.org/10.1016/0960-1686(91)90050-H

Formenti, P., D'Anna, B., Flamant, C., Mallet, M., Piketh, S. J., Schepanski, K., Waquet, F., Auriol, F., Brogniez, G., Burnet, F., Chaboureau, J.-P., Chauvigné, A., Chazette, P., Denjean, C., Desboeufs, K., Doussin, J.-F., Elguindi, N., Feuerstein, S., Gaetani, M.,…Holben, B. (2019). The Aerosols,

Radiation and Clouds in Southern Africa Field Campaign in Namibia: Overview, Illustrative Observations, and Way Forward. *Bulletin of the American Meteorological Society*, *100*(7), 1277-1298. https://doi.org/10.1175/bams-d-17-0278.1

Fountoukis, C., & Nenes, A. (2005). Continued development of a cloud droplet formation parameterization for global climate models. *Journal of Geophysical Research: Atmospheres*, *110*(D11). https://doi.org/https://doi.org/10.1029/2004JD005591

Giles, D. M., Sinyuk, A., Sorokin, M. G., Schafer, J. S., Smirnov, A., Slutsker, I., Eck, T. F., Holben, B. N., Lewis, J. R., Campbell, J. R., Welton, E. J., Korkin, S. V., & Lyapustin, A. I. (2019). Advancements in the Aerosol Robotic Network (AERONET) Version 3 database – automated near-real-time quality control algorithm with improved cloud screening for Sun photometer aerosol optical depth (AOD) measurements. *Atmos. Meas. Tech.*, *12*(1), 169-209. https://doi.org/10.5194/amt-12-169-2019

Granier, C., Bessagnet, B., Bond, T., D'Angiola, A., Denier van der Gon, H., Frost, G. J., Heil, A., Kaiser, J. W., Kinne, S., Klimont, Z., Kloster, S., Lamarque, J.-F., Liousse, C., Masui, T., Meleux, F., Mieville, A., Ohara, T., Raut, J.-C., Riahi, K.,…van Vuuren, D. P. (2011). Evolution of anthropogenic and biomass burning emissions of air pollutants at global and regional scales during the 1980–2010 period. *Climatic Change*, *109*(1), 163. https://doi.org/10.1007/s10584-011-0154-1

Grell, G. A., Peckham, S. E., Schmitz, R., McKeen, S. A., Frost, G., Skamarock, W. C., & Eder, B. (2005). Fully coupled "online" chemistry within the WRF model. *Atmospheric Environment*, *39*(37), 6957-6975. https://doi.org/https://doi.org/10.1016/j.atmosenv.2005.04.027

Hansen, J., Sato, M., & Ruedy, R. (1997). Radiative forcing and climate response. *Journal of Geophysical Research: Atmospheres*, *102*(D6), 6831-6864. https://doi.org/https://doi.org/10.1029/96JD03436

Haywood, J. M., Abel, S. J., Barrett, P. A., Bellouin, N., Blyth, A., Bower, K. N., Brooks, M., Carslaw, K., Che, H., Coe, H., Cotterell, M. I., Crawford, I., Cui, Z., Davies, N., Dingley, B., Field, P., Formenti, P., Gordon, H., de Graaf, M.,…Zuidema, P. (2021). The CLoud–Aerosol–Radiation Interaction and Forcing: Year 2017 (CLARIFY-2017) measurement campaign. *Atmos. Chem. Phys.*, *21*(2), 1049-1084. https://doi.org/10.5194/acp-21-1049-2021

Haywood, J. M., Osborne, S. R., Francis, P. N., Keil, A., Formenti, P., Andreae, M. O., & Kaye, P. H. (2003). The mean physical and optical properties of regional haze dominated by biomass burning aerosol measured from the C-130 aircraft during SAFARI 2000. *Journal of Geophysical Research: Atmospheres*, *108*(D13). https://doi.org/https://doi.org/10.1029/2002JD002226

Haywood, J. M., & Shine, K. P. (1997). Multi-spectral calculations of the direct radiative forcing of tropospheric sulphate and soot aerosols using a column model. *Quarterly Journal of the Royal Meteorological Society*, *123*(543), 1907-1930. https://doi.org/https://doi.org/10.1002/qj.49712354307

Hodshire, A. L., Akherati, A., Alvarado, M. J., Brown-Steiner, B., Jathar, S. H., Jimenez, J. L., Kreidenweis, S. M., Lonsdale, C. R., Onasch, T. B., Ortega, A. M., & Pierce, J. R. (2019). Aging Effects on Biomass Burning Aerosol Mass and Composition: A Critical Review of Field and Laboratory Studies. *Environmental Science & Technology*, *53*(17), 10007-10022. https://doi.org/10.1021/acs.est.9b02588

Holanda, B. A., Pöhlker, M. L., Walter, D., Saturno, J., Sörgel, M., Ditas, J., Ditas, F., Schulz, C., Franco, M. A., Wang, Q., Donth, T., Artaxo, P., Barbosa, H. M. J., Borrmann, S., Braga, R., Brito, J., Cheng, Y., Dollner, M., Kaiser, J. W.,…Pöhlker, C. (2020). Influx of African biomass burning aerosol during the Amazonian dry season through layered transatlantic transport of black carbon-rich smoke. *Atmos. Chem. Phys.*, *20*(8), 4757-4785. https://doi.org/10.5194/acp-20-4757-2020

Holben, B. N., Eck, T. F., Slutsker, I., Tanré, D., Buis, J. P., Setzer, A., Vermote, E., Reagan, J. A., Kaufman, Y. J., Nakajima, T., Lavenu, F., Jankowiak, I., & Smirnov, A. (1998). AERONET—A Federated

Instrument Network and Data Archive for Aerosol Characterization. *Remote Sensing of Environment*, *66*(1), 1-16. https://doi.org/https://doi.org/10.1016/S0034-4257(98)00031-5

Hopkins, R. J., Lewis, K., Desyaterik, Y., Wang, Z., Tivanski, A. V., Arnott, W. P., Laskin, A., & Gilles, M. K. (2007). Correlations between optical, chemical and physical properties of biomass burn aerosols. *Geophysical Research Letters*, *34*(18). https://doi.org/https://doi.org/10.1029/2007GL030502

Howes, C., Saide, P. E., Coe, H., Dobracki, A., Freitag, S., Haywood, J. M., Howell, S. G., Gupta, S., Uin, J., Kacarab, M., Kuang, C., Leung, L. R., Nenes, A., McFarquhar, G. M., Podolske, J., Redemann, J., Sedlacek, A. J., Thornhill, K. L., Wong, J. P. S.,…Zuidema, P. (2023). Biomass-burning smoke's properties and its interactions with marine stratocumulus clouds in WRF-CAM5 and southeastern Atlantic field campaigns. *Atmos. Chem. Phys.*, *23*(21), 13911-13940. https://doi.org/10.5194/acp-23-13911-2023

Jen, C. N., Hatch, L. E., Selimovic, V., Yokelson, R. J., Weber, R., Fernandez, A. E., Kreisberg, N. M., Barsanti, K. C., & Goldstein, A. H. (2019). Speciated and total emission factors of particulate organics from burning western US wildland fuels and their dependence on combustion efficiency. *Atmos. Chem. Phys.*, *19*(2), 1013-1026. https://doi.org/10.5194/acp-19-1013-2019

Jimenez, J. L., Canagaratna, M. R., Donahue, N. M., Prevot, A. S. H., Zhang, Q., Kroll, J. H., DeCarlo, P. F., Allan, J. D., Coe, H., Ng, N. L., Aiken, A. C., Docherty, K. S., Ulbrich, I. M., Grieshop, A. P., Robinson, A. L., Duplissy, J., Smith, J. D., Wilson, K. R., Lanz, V. A.,…Worsnop, D. R. (2009). Evolution of Organic Aerosols in the Atmosphere. *Science*, *326*(5959), 1525-1529. https://doi.org/doi:10.1126/science.1180353

Jones, M. W., Abatzoglou, J. T., Veraverbeke, S., Andela, N., Lasslop, G., Forkel, M., Smith, A. J. P., Burton, C., Betts, R. A., van der Werf, G. R., Sitch, S., Canadell, J. G., Santín, C., Kolden, C., Doerr, S. H., & Le Quéré, C. (2022). Global and Regional Trends and Drivers of Fire Under Climate Change. *Reviews of Geophysics*, *60*(3), e2020RG000726. https://doi.org/https://doi.org/10.1029/2020RG000726

Keil, A., & Haywood, J. M. (2003). Solar radiative forcing by biomass burning aerosol particles during SAFARI 2000: A case study based on measured aerosol and cloud properties. *Journal of Geophysical Research: Atmospheres*, *108*(D13). https://doi.org/https://doi.org/10.1029/2002JD002315

Keywood, M., Kanakidou, M., Stohl, A., Dentener, F., Grassi, G., Meyer, C. P., Torseth, K., Edwards, D., Thompson, A. M., Lohmann, U., & Burrows, J. (2013). Fire in the Air: Biomass Burning Impacts in a Changing Climate. *Critical Reviews in Environmental Science and Technology*, *43*(1), 40-83. https://doi.org/10.1080/10643389.2011.604248

Kleinman, L. I., Sedlacek Iii, A. J., Adachi, K., Buseck, P. R., Collier, S., Dubey, M. K., Hodshire, A. L., Lewis, E., Onasch, T. B., Pierce, J. R., Shilling, J., Springston, S. R., Wang, J., Zhang, Q., Zhou, S., & Yokelson, R. J. (2020). Rapid evolution of aerosol particles and their optical properties downwind of wildfires in the western US. *Atmos. Chem. Phys.*, *20*(21), 13319-13341. https://doi.org/10.5194/acp-20-13319-2020

Koch, D., & Del Genio, A. D. (2010). Black carbon semi-direct effects on cloud cover: review and synthesis. *Atmos. Chem. Phys.*, *10*(16), 7685-7696. https://doi.org/10.5194/acp-10-7685-2010

Konovalov, I. B., Golovushkin, N. A., Beekmann, M., & Andreae, M. O. (2021). Insights into the aging of biomass burning aerosol from satellite observations and 3D atmospheric modeling: evolution of the aerosol optical properties in Siberian wildfire plumes. *Atmos. Chem. Phys.*, *21*(1), 357-392. https://doi.org/10.5194/acp-21-357-2021

Lack, D. A., & Cappa, C. D. (2010). Impact of brown and clear carbon on light absorption enhancement, single scatter albedo and absorption wavelength dependence of black carbon. *Atmos. Chem. Phys.*, *10*(9), 4207-4220. https://doi.org/10.5194/acp-10-4207-2010

Laskin, A., Laskin, J., & Nizkorodov, S. A. (2015). Chemistry of Atmospheric Brown Carbon. *Chemical Reviews*, *115*(10), 4335-4382. https://doi.org/10.1021/cr5006167

Leahy, L. V., Anderson, T. L., Eck, T. F., & Bergstrom, R. W. (2007). A synthesis of single scattering albedo of biomass burning aerosol over southern Africa during SAFARI 2000. *Geophysical Research Letters*, *34*(12). https://doi.org/https://doi.org/10.1029/2007GL029697

LeBlanc, S. E., Pilewskie, P., Schmidt, K. S., & Coddington, O. (2015). A spectral method for discriminating thermodynamic phase and retrieving cloud optical thickness and effective radius using transmitted solar radiance spectra. *Atmos. Meas. Tech.*, *8*(3), 1361-1383. https://doi.org/10.5194/amt-8-1361-2015

LeBlanc, S. E., Redemann, J., Flynn, C., Pistone, K., Kacenelenbogen, M., Segal-Rosenheimer, M., Shinozuka, Y., Dunagan, S., Dahlgren, R. P., Meyer, K., Podolske, J., Howell, S. G., Freitag, S., Small-Griswold, J., Holben, B., Diamond, M., Wood, R., Formenti, P., Piketh, S.,…Namwoonde, A. (2020). Above-cloud aerosol optical depth from airborne observations in the southeast Atlantic. *Atmos. Chem. Phys.*, *20*(3), 1565-1590. https://doi.org/10.5194/acp-20-1565-2020

Lenhardt, E. D., Gao, L., Redemann, J., Xu, F., Burton, S. P., Cairns, B., Chang, I., Ferrare, R. A., Hostetler, C. A., Saide, P. E., Howes, C., Shinozuka, Y., Stamnes, S., Kacarab, M., Dobracki, A., Wong, J., Freitag, S., & Nenes, A. (2023). Use of lidar aerosol extinction and backscatter coefficients to estimate cloud condensation nuclei (CCN) concentrations in the southeast Atlantic. *Atmos. Meas. Tech.*, *16*(7), 2037-2054. https://doi.org/10.5194/amt-16-2037-2023

Levin, E. J. T., McMeeking, G. R., Carrico, C. M., Mack, L. E., Kreidenweis, S. M., Wold, C. E., Moosmüller, H., Arnott, W. P., Hao, W. M., Collett Jr., J. L., & Malm, W. C. (2010). Biomass burning smoke aerosol properties measured during Fire Laboratory at Missoula Experiments (FLAME). *Journal of Geophysical Research: Atmospheres*, *115*(D18). https://doi.org/https://doi.org/10.1029/2009JD013601

Lim, K.-S. S., Fan, J., Leung, L. R., Ma, P.-L., Singh, B., Zhao, C., Zhang, Y., Zhang, G., & Song, X. (2014). Investigation of aerosol indirect effects using a cumulus microphysics parameterization in a regional climate model. *Journal of Geophysical Research: Atmospheres*, *119*(2), 906-926. https://doi.org/https://doi.org/10.1002/2013JD020958

Liu, D., Li, S., Hu, D., Kong, S., Cheng, Y., Wu, Y., Ding, S., Hu, K., Zheng, S., Yan, Q., Zheng, H., Zhao, D., Tian, P., Ye, J., Huang, M., & Ding, D. (2021). Evolution of Aerosol Optical Properties from Wood Smoke in Real Atmosphere Influenced by Burning Phase and Solar Radiation. *Environmental Science & Technology*, *55*(9), 5677-5688. https://doi.org/10.1021/acs.est.0c07569

Liu, S., Aiken, A. C., Arata, C., Dubey, M. K., Stockwell, C. E., Yokelson, R. J., Stone, E. A., Jayarathne, T., Robinson, A. L., DeMott, P. J., & Kreidenweis, S. M. (2014). Aerosol single scattering albedo dependence on biomass combustion efficiency: Laboratory and field studies. *Geophysical Research Letters*, *41*(2), 742-748. https://doi.org/10.1002/2013gl058392

Liu, X., Easter, R. C., Ghan, S. J., Zaveri, R., Rasch, P., Shi, X., Lamarque, J. F., Gettelman, A., Morrison, H., Vitt, F., Conley, A., Park, S., Neale, R., Hannay, C., Ekman, A. M. L., Hess, P., Mahowald, N., Collins, W., Iacono, M. J.,…Mitchell, D. (2012). Toward a minimal representation of aerosols in climate models: description and evaluation in the Community Atmosphere Model CAM5. *Geosci. Model Dev.*, *5*(3), 709-739. https://doi.org/10.5194/gmd-5-709-2012

Ma, P.-L., Rasch, P. J., Fast, J. D., Easter, R. C., Gustafson Jr, W., Liu, X., Ghan, S. J., & Singh, B. (2014). Assessing the CAM5 physics suite in the WRF-Chem model: Implementation, resolution sensitivity, and a first evaluation for a regional case study. *Geoscientific Model Development*, *7*(3), 755-778.

Mallet, M., Solmon, F., Nabat, P., Elguindi, N., Waquet, F., Bouniol, D., Sayer, A. M., Meyer, K., Roehrig, R., Michou, M., Zuidema, P., Flamant, C., Redemann, J., & Formenti, P. (2020). Direct and semi-direct radiative forcing of biomass-burning aerosols over the southeast Atlantic (SEA) and its

sensitivity to absorbing properties: a regional climate modeling study. *Atmos. Chem. Phys.*, *20*(21), 13191-13216. https://doi.org/10.5194/acp-20-13191-2020

Meyer, K., Platnick, S., Oreopoulos, L., & Lee, D. (2013). Estimating the direct radiative effect of absorbing aerosols overlying marine boundary layer clouds in the southeast Atlantic using MODIS and CALIOP. *Journal of Geophysical Research: Atmospheres*, *118*(10), 4801-4815. https://doi.org/https://doi.org/10.1002/jgrd.50449

Mishra, A. K., Koren, I., & Rudich, Y. (2015). Effect of aerosol vertical distribution on aerosol-radiation interaction: A theoretical prospect. *Heliyon*, *1*(2), e00036. https://doi.org/https://doi.org/10.1016/j.heliyon.2015.e00036

Mitchell, L. T., Redemann, J., Pistone, K., LeBlanc, S., & Schmidt, S. (2023). *Subseasonal and Spatial Variability of Biomass Burning Aerosol Radiative Properties Observed over the Southeast Atlantic during ORACLES 2016-2018 by 4STAR, In-Situ, and the Southern African AERONET Extended Record* AGU23, San Francisco, CA.

Moosmüller, H., Engelbrecht, J. P., Skiba, M., Frey, G., Chakrabarty, R. K., & Arnott, W. P. (2012). Single scattering albedo of fine mineral dust aerosols controlled by iron concentration. *Journal of Geophysical Research: Atmospheres*, *117*(D11). https://doi.org/https://doi.org/10.1029/2011JD016909

Morrison, H., & Gettelman, A. (2008). A New Two-Moment Bulk Stratiform Cloud Microphysics Scheme in the Community Atmosphere Model, Version 3 (CAM3). Part I: Description and Numerical Tests. *Journal of Climate*, *21*(15), 3642-3659. https://doi.org/10.1175/2008jcli2105.1

Nascimento, J. P., Bela, M. M., Meller, B. B., Banducci, A. L., Rizzo, L. V., Vara-Vela, A. L., Barbosa, H. M. J., Gomes, H., Rafee, S. A. A., Franco, M. A., Carbone, S., Cirino, G. G., Souza, R. A. F., McKeen, S. A., & Artaxo, P. (2021). Aerosols from anthropogenic and biogenic sources and their interactions – modeling aerosol formation, optical properties, and impacts over the central Amazon basin. *Atmos. Chem. Phys.*, *21*(9), 6755-6779. https://doi.org/10.5194/acp-21-6755-2021

Niemand, M., Möhler, O., Vogel, B., Vogel, H., Hoose, C., Connolly, P., Klein, H., Bingemer, H., DeMott, P., Skrotzki, J., & Leisner, T. (2012). A Particle-Surface-Area-Based Parameterization of Immersion Freezing on Desert Dust Particles. *Journal of the Atmospheric Sciences*, *69*(10), 3077-3092. https://doi.org/10.1175/jas-d-11-0249.1

ORACLES. (2020). *ORACLES Science Team. ObseRvations of Aerosols above CLouds and their intEractionS.* (https://doi.org/https://doi.org/10.5067/SUBORBITAL/ORACLES/DATA001

Pistone, K., Redemann, J., Doherty, S., Zuidema, P., Burton, S., Cairns, B., Cochrane, S., Ferrare, R., Flynn, C., Freitag, S., Howell, S. G., Kacenelenbogen, M., LeBlanc, S., Liu, X., Schmidt, K. S., Sedlacek Iii, A. J., Segal-Rozenhaimer, M., Shinozuka, Y., Stamnes, S.,…Xu, F. (2019). Intercomparison of biomass burning aerosol optical properties from in situ and remote-sensing instruments in ORACLES-2016. *Atmos. Chem. Phys.*, *19*(14), 9181-9208. https://doi.org/10.5194/acp-19-9181-2019

Pósfai, M., Anderson, J. R., Buseck, P. R., & Sievering, H. (1995). Compositional variations of sea-salt-mode aerosol particles from the North Atlantic. *Journal of Geophysical Research: Atmospheres*, *100*(D11), 23063-23074. https://doi.org/https://doi.org/10.1029/95JD01636

Queface, A. J., Piketh, S. J., Eck, T. F., Tsay, S.-C., & Mavume, A. F. (2011). Climatology of aerosol optical properties in Southern Africa. *Atmospheric Environment*, *45*(17), 2910-2921. https://doi.org/https://doi.org/10.1016/j.atmosenv.2011.01.056

Redemann, J., Russell, P. B., & Hamill, P. (2001). Dependence of aerosol light absorption and single-scattering albedo on ambient relative humidity for sulfate aerosols with black carbon cores. *Journal of Geophysical Research: Atmospheres*, *106*(D21), 27485-27495. https://doi.org/https://doi.org/10.1029/2001JD900231

Redemann, J., Wood, R., Zuidema, P., Doherty, S. J., Luna, B., LeBlanc, S. E., Diamond, M. S., Shinozuka, Y., Chang, I. Y., Ueyama, R., Pfister, L., Ryoo, J. M., Dobracki, A. N., da Silva, A. M., Longo, K. M., Kacenelenbogen, M. S., Flynn, C. J., Pistone, K., Knox, N. M.,…Gao, L. (2021). An overview of the ORACLES (ObseRvations of Aerosols above CLouds and their intEractionS) project: aerosol–cloud–radiation interactions in the southeast Atlantic basin. *Atmos. Chem. Phys.*, *21*(3), 1507-1563. https://doi.org/10.5194/acp-21-1507-2021

Reid, J. S., Hobbs, P. V., Ferek, R. J., Blake, D. R., Martins, J. V., Dunlap, M. R., & Liousse, C. (1998). Physical, chemical, and optical properties of regional hazes dominated by smoke in Brazil. *Journal of Geophysical Research: Atmospheres*, *103*(D24), 32059-32080. https://doi.org/https://doi.org/10.1029/98JD00458

Ryoo, J. M., Pfister, L., Ueyama, R., Zuidema, P., Wood, R., Chang, I., & Redemann, J. (2021). A meteorological overview of the ORACLES (ObseRvations of Aerosols above CLouds and their intEractionS) campaign over the southeastern Atlantic during 2016–2018: Part 1 – Climatology. *Atmos. Chem. Phys.*, *21*(22), 16689-16707. https://doi.org/10.5194/acp-21-16689-2021

Saide, P. E., Thompson, G., Eidhammer, T., da Silva, A. M., Pierce, R. B., & Carmichael, G. R. (2016). Assessment of biomass burning smoke influence on environmental conditions for multi-year tornado outbreaks by combining aerosol-aware microphysics and fire emission constraints. *J Geophys Res Atmos*, *121*(17), 10294-10311. https://doi.org/10.1002/2016JD025056

Sakaeda, N., Wood, R., & Rasch, P. J. (2011). Direct and semidirect aerosol effects of southern African biomass burning aerosol. *Journal of Geophysical Research: Atmospheres*, *116*(D12). https://doi.org/https://doi.org/10.1029/2010JD015540

Saleh, R., Marks, M., Heo, J., Adams, P. J., Donahue, N. M., & Robinson, A. L. (2015). Contribution of brown carbon and lensing to the direct radiative effect of carbonaceous aerosols from biomass and biofuel burning emissions. *Journal of Geophysical Research: Atmospheres*, *120*(19), 10,285-210,296. https://doi.org/https://doi.org/10.1002/2015JD023697

Samset, B. H., Stjern, C. W., Andrews, E., Kahn, R. A., Myhre, G., Schulz, M., & Schuster, G. L. (2018). Aerosol Absorption: Progress Towards Global and Regional Constraints. *Current Climate Change Reports*, *4*(2), 65-83. https://doi.org/10.1007/s40641-018-0091-4

Santer, B. D., Taylor, K. E., Wigley, T. M. L., Johns, T. C., Jones, P. D., Karoly, D. J., Mitchell, J. F. B., Oort, A. H., Penner, J. E., Ramaswamy, V., Schwarzkopf, M. D., Stouffer, R. J., & Tett, S. (1996). A search for human influences on the thermal structure of the atmosphere. *Nature*, *382*(6586), 39-46. https://doi.org/10.1038/382039a0

Satheesh, S. K., Vinoj, V., & Krishna Moorthy, K. (2010). Radiative effects of aerosols at an urban location in southern India: Observations versus model. *Atmospheric Environment*, *44*(39), 5295-5304. https://doi.org/https://doi.org/10.1016/j.atmosenv.2010.07.020

Schuster, G. L., Dubovik, O., & Holben, B. N. (2006). Angstrom exponent and bimodal aerosol size distributions. *Journal of Geophysical Research: Atmospheres*, *111*(D7). https://doi.org/https://doi.org/10.1029/2005JD006328

Sedlacek, A. J., III, Lewis, E. R., Onasch, T. B., Zuidema, P., Redemann, J., Jaffe, D., & Kleinman, L. I. (2022). Using the Black Carbon Particle Mixing State to Characterize the Lifecycle of Biomass Burning Aerosols. *Environmental Science & Technology*, *56*(20), 14315-14325. https://doi.org/10.1021/acs.est.2c03851

Segal-Rosenheimer, M., Russell, P. B., Schmid, B., Redemann, J., Livingston, J. M., Flynn, C. J., Johnson, R. R., Dunagan, S. E., Shinozuka, Y., Herman, J., Cede, A., Abuhassan, N., Comstock, J. M., Hubbe, J. M., Zelenyuk, A., & Wilson, J. (2014). Tracking elevated pollution layers with a newly developed hyperspectral Sun/Sky spectrometer (4STAR): Results from the TCAP 2012 and 2013 campaigns. *Journal of Geophysical Research: Atmospheres*, *119*(5), 2611-2628. https://doi.org/https://doi.org/10.1002/2013JD020884

Seidel, D. J., Ao, C. O., & Li, K. (2010). Estimating climatological planetary boundary layer heights from radiosonde observations: Comparison of methods and uncertainty analysis. *Journal of Geophysical Research: Atmospheres*, *115*(D16). https://doi.org/https://doi.org/10.1029/2009JD013680

Shinozuka, Y., Kacenelenbogen, M. S., Burton, S. P., Howell, S. G., Zuidema, P., Ferrare, R. A., LeBlanc, S. E., Pistone, K., Broccardo, S., Redemann, J., Schmidt, K. S., Cochrane, S. P., Fenn, M., Freitag, S., Dobracki, A., Segal-Rosenheimer, M., & Flynn, C. J. (2020b). Daytime aerosol optical depth above low-level clouds is similar to that in adjacent clear skies at the same heights: airborne observation above the southeast Atlantic. *Atmos. Chem. Phys.*, *20*(19), 11275-11285. https://doi.org/10.5194/acp-20-11275-2020

Shinozuka, Y., Saide, P. E., Ferrada, G. A., Burton, S. P., Ferrare, R., Doherty, S. J., Gordon, H., Longo, K., Mallet, M., Feng, Y., Wang, Q., Cheng, Y., Dobracki, A., Freitag, S., Howell, S. G., LeBlanc, S., Flynn, C., Segal-Rosenhaimer, M., Pistone, K.,…Zuidema, P. (2020a). Modeling the smoky troposphere of the southeast Atlantic: a comparison to ORACLES airborne observations from September of 2016. *Atmos. Chem. Phys.*, *20*(19), 11491-11526. https://doi.org/10.5194/acp-20-11491-2020

Sinyuk, A., Holben, B. N., Eck, T. F., Giles, D. M., Slutsker, I., Korkin, S., Schafer, J. S., Smirnov, A., Sorokin, M., & Lyapustin, A. (2020). The AERONET Version 3 aerosol retrieval algorithm, associated uncertainties and comparisons to Version 2. *Atmos. Meas. Tech.*, *13*(6), 3375-3411. https://doi.org/10.5194/amt-13-3375-2020

Smirnov, A., Holben, B. N., Kaufman, Y. J., Dubovik, O., Eck, T. F., Slutsker, I., Pietras, C., & Halthore, R. N. (2002). Optical Properties of Atmospheric Aerosol in Maritime Environments. *Journal of the Atmospheric Sciences*, *59*(3), 501-523. https://doi.org/https://doi.org/10.1175/1520-0469(2002)059<0501:OPOAAI>2.0.CO;2

Song, X., & Zhang, G. J. (2011). Microphysics parameterization for convective clouds in a global climate model: Description and single-column model tests. *Journal of Geophysical Research: Atmospheres*, *116*(D2). https://doi.org/https://doi.org/10.1029/2010JD014833

Stein, A. F., Draxler, R. R., Rolph, G. D., Stunder, B. J. B., Cohen, M. D., & Ngan, F. (2015). NOAA's HYSPLIT Atmospheric Transport and Dispersion Modeling System. *Bulletin of the American Meteorological Society*, *96*(12), 2059-2077. https://doi.org/https://doi.org/10.1175/BAMS-D-14-00110.1

Stier, P., Schutgens, N. A. J., Bellouin, N., Bian, H., Boucher, O., Chin, M., Ghan, S., Huneeus, N., Kinne, S., Lin, G., Ma, X., Myhre, G., Penner, J. E., Randles, C. A., Samset, B., Schulz, M., Takemura, T., Yu, F., Yu, H., & Zhou, C. (2013). Host model uncertainties in aerosol radiative forcing estimates: results from the AeroCom Prescribed intercomparison study. *Atmos. Chem. Phys.*, *13*(6), 3245-3270. https://doi.org/10.5194/acp-13-3245-2013

Takemura, T., Nakajima, T., Dubovik, O., Holben, B. N., & Kinne, S. (2002). Single-Scattering Albedo and Radiative Forcing of Various Aerosol Species with a Global Three-Dimensional Model. *Journal of Climate*, *15*(4), 333-352. https://doi.org/https://doi.org/10.1175/1520-0442(2002)015<0333:SSAARF>2.0.CO;2

Tatro, T., & Zuidema, P. (2025). More biomass burning aerosol is being advected westward over the southern tropical Atlantic since 2003. *Science of The Total Environment*, *965*, 178506. https://doi.org/https://doi.org/10.1016/j.scitotenv.2025.178506

Thompson, G., & Eidhammer, T. (2014). A Study of Aerosol Impacts on Clouds and Precipitation Development in a Large Winter Cyclone. *Journal of the Atmospheric Sciences*, *71*(10), 3636-3658. https://doi.org/10.1175/jas-d-13-0305.1

Twomey, S. (1974). Pollution and the planetary albedo. *Atmospheric Environment (1967)*, *8*(12), 1251-1256. https://doi.org/https://doi.org/10.1016/0004-6981(74)90004-3

Twomey, S. (1977). The Influence of Pollution on the Shortwave Albedo of Clouds. *Journal of Atmospheric Sciences*, *34*(7), 1149-1152. https://doi.org/10.1175/1520-0469(1977)034<1149:Tiopot>2.0.Co;2

Vakkari, V., Beukes, J. P., Dal Maso, M., Aurela, M., Josipovic, M., & van Zyl, P. G. (2018). Major secondary aerosol formation in southern African open biomass burning plumes. *Nature Geoscience*, *11*(8), 580-583. https://doi.org/10.1038/s41561-018-0170-0

van der Werf, G. R., Randerson, J. T., Giglio, L., Collatz, G. J., Mu, M., Kasibhatla, P. S., Morton, D. C., DeFries, R. S., Jin, Y., & van Leeuwen, T. T. (2010). Global fire emissions and the contribution of deforestation, savanna, forest, agricultural, and peat fires (1997–2009). *Atmos. Chem. Phys.*, *10*(23), 11707-11735. https://doi.org/10.5194/acp-10-11707-2010

Vermote, E., Ellicott, E., Dubovik, O., Lapyonok, T., Chin, M., Giglio, L., & Roberts, G. J. (2009). An approach to estimate global biomass burning emissions of organic and black carbon from MODIS fire radiative power. *Journal of Geophysical Research: Atmospheres*, *114*(D18). https://doi.org/https://doi.org/10.1029/2008JD011188

Wang, Y., Vogel, J. M., Lin, Y., Pan, B., Hu, J., Liu, Y., Dong, X., Jiang, J. H., Yung, Y. L., & Zhang, R. (2018). Aerosol microphysical and radiative effects on continental cloud ensembles. *Advances in Atmospheric Sciences*, *35*(2), 234-247. https://doi.org/10.1007/s00376-017-7091-5

Waquet, F., Peers, F., Ducos, F., Goloub, P., Platnick, S., Riedi, J., Tanré, D., & Thieuleux, F. (2013). Global analysis of aerosol properties above clouds. *Geophysical Research Letters*, *40*(21), 5809-5814. https://doi.org/https://doi.org/10.1002/2013GL057482

Wilcox, E. M. (2010). Stratocumulus cloud thickening beneath layers of absorbing smoke aerosol. *Atmos. Chem. Phys.*, *10*(23), 11769-11777. https://doi.org/10.5194/acp-10-11769-2010

Wilcox, E. M. (2012). Direct and semi-direct radiative forcing of smoke aerosols over clouds. *Atmos. Chem. Phys.*, *12*(1), 139-149. https://doi.org/10.5194/acp-12-139-2012

Wu, H., Taylor, J. W., Szpek, K., Langridge, J. M., Williams, P. I., Flynn, M., Allan, J. D., Abel, S. J., Pitt, J., Cotterell, M. I., Fox, C., Davies, N. W., Haywood, J., & Coe, H. (2020). Vertical variability of the properties of highly aged biomass burning aerosol transported over the southeast Atlantic during CLARIFY-2017. *Atmos. Chem. Phys.*, *20*(21), 12697-12719. https://doi.org/10.5194/acp-20-12697-2020

Zaveri, R. A., & Peters, L. K. (1999). A new lumped structure photochemical mechanism for large-scale applications. *Journal of Geophysical Research: Atmospheres*, *104*(D23), 30387-30415. https://doi.org/https://doi.org/10.1029/1999JD900876

Zhang, G. J., & McFarlane, N. A. (1995). Sensitivity of climate simulations to the parameterization of cumulus convection in the Canadian climate centre general circulation model. *Atmosphere-Ocean*, *33*(3), 407-446. https://doi.org/10.1080/07055900.1995.9649539

Zhang, J., & Zuidema, P. (2019). The diurnal cycle of the smoky marine boundary layer observed during August in the remote southeast Atlantic. *Atmos. Chem. Phys.*, *19*(23), 14493-14516. https://doi.org/10.5194/acp-19-14493-2019

Zhang, J., & Zuidema, P. (2021). Sunlight-absorbing aerosol amplifies the seasonal cycle in low-cloud fraction over the southeast Atlantic. *Atmos. Chem. Phys.*, *21*(14), 11179-11199. https://doi.org/10.5194/acp-21-11179-2021

Zhang, Y., Chen, Y., Fan, J., & Leung, L.-Y. R. (2015b). Application of an Online-Coupled Regional Climate Model, WRF-CAM5, over East Asia for Examination of Ice Nucleation Schemes: Part II. Sensitivity to Heterogeneous Ice Nucleation Parameterizations and Dust Emissions. *Climate*, *3*(3), 753-774. https://www.mdpi.com/2225-1154/3/3/753

Zhang, Y., Zhang, X., Wang, K., He, J., Leung, L. R., Fan, J., & Nenes, A. (2015a). Incorporating an advanced aerosol activation parameterization into WRF-CAM5: Model evaluation and

parameterization intercomparison. *Journal of Geophysical Research: Atmospheres*, *120*(14), 6952-6979. https://doi.org/https://doi.org/10.1002/2014JD023051

Zhou, S., Collier, S., Jaffe, D. A., Briggs, N. L., Hee, J., Sedlacek Iii, A. J., Kleinman, L., Onasch, T. B., & Zhang, Q. (2017). Regional influence of wildfires on aerosol chemistry in the western US and insights into atmospheric aging of biomass burning organic aerosol. *Atmos. Chem. Phys.*, *17*(3), 2477-2493. https://doi.org/10.5194/acp-17-2477-2017

Zuidema, P., Redemann, J., Haywood, J., Wood, R., Piketh, S., Hipondoka, M., & Formenti, P. (2016). Smoke and Clouds above the Southeast Atlantic: Upcoming Field Campaigns Probe Absorbing Aerosol's Impact on Climate. *Bulletin of the American Meteorological Society*, *97*(7), 1131-1135. https://doi.org/10.1175/bams-d-15-00082.1

Zuidema, P., Sedlacek III, A. J., Flynn, C., Springston, S., Delgadillo, R., Zhang, J., Aiken, A. C., Koontz, A., & Muradyan, P. (2018). The Ascension Island Boundary Layer in the Remote Southeast Atlantic is Often Smoky. *Geophysical Research Letters*, *45*(9), 4456-4465. https://doi.org/https://doi.org/10.1002/2017GL076926